

Sneutrino as Lightest Supersymmetric Particle in B_3 mSUGRA Models and Signals at the LHC

M. A. Bernhardt*, S. P. Das†, H. K. Dreiner‡, and S. Grab§
Physikalisches Institut, Nußallee 12, University of Bonn, 53115 Bonn, Germany

We consider B_3 mSUGRA models where we have one lepton number violating $L_i Q_j \bar{D}_k$ operator at the GUT scale. This can alter the supersymmetric mass spectrum leading to a sneutrino as the lightest supersymmetric particle in a large region of parameter space. We take into account the restrictions from neutrino masses, the muon anomalous magnetic moment, $b \rightarrow s\gamma$ and other precision measurements. We furthermore investigate existing restrictions from direct searches at LEP, the Tevatron and the CERN $p\bar{p}$ collider. We then give examples for characteristic signatures at the LHC.

I. INTRODUCTION

Supersymmetry (SUSY) [1] is a promising extension of the Standard Model of particle physics (SM) [2]; the simplest form is denoted the supersymmetric SM (SSM). It should be imminently testable at the LHC [3]. Supersymmetric particles, if they exist, typically decay instantaneously on collider time scales down to the lightest supersymmetric particle (LSP). The nature and possible decay properties of the LSP are thus an essential ingredient for all SUSY signatures. In the minimal SSM, with conserved proton-hexality, P_6 , [4] (or equivalently conserved R-parity [5]), the LSP is stable. Cosmological constraints as well as LEP searches then restrict the LSP to be the lightest neutralino [6, 7].

If we allow for violation of proton-hexality, the LSP is no longer stable and in general any supersymmetric particle can be the LSP [8]. However, it is impossible to perform a detailed phenomenological study of the corresponding wide variety of mass orderings of the sparticle spectrum. We thus must restrict ourselves to well motivated models. In this paper, we focus on the B_3 minimal supergravity (mSUGRA) model [9]. In Ref. [9, 10] it was shown that in such models there are three different LSP candidates: the lightest neutralino, $\tilde{\chi}_1^0$, the lightest scalar tau (stau), $\tilde{\tau}_1$ and the sneutrino, $\tilde{\nu}_i$. The lightest neutralino LSP has been studied extensively in the literature, see for example [11, 12, 13, 14]. More recently the stau LSP has also been investigated [9, 10, 15, 16, 17, 18, 19].

In this paper we consider in detail the case of a $\tilde{\nu}_i$ LSP. The $\tilde{\nu}_i$ is special, because unlike the $\tilde{\chi}_1^0$ and $\tilde{\tau}_1$, the B_3 contributions to the renormalization group equations (RGEs) are essential for it to become the LSP. In Ref. [10] only one example B_3 mSUGRA scenario with a $\tilde{\nu}_\tau$ LSP was presented. We go beyond this work and systematically investigate the B_3 mSUGRA pa-

rameter space with a $\tilde{\nu}_i$ LSP. In the first part of our paper we analyse, which conditions at the grand unification (GUT) scale lead to a $\tilde{\nu}_i$ LSP. In the second part, we point out striking collider signatures at the LHC which can lead to a SUSY discovery and which can distinguish a $\tilde{\nu}_i$ LSP scenario from a “standard” mSUGRA scenario with a stable $\tilde{\chi}_1^0$ LSP.

The outline of our paper is as follows. In Sect. II, we briefly review the P_6 and B_3 mSUGRA models and discuss the RGEs which lead to a $\tilde{\nu}_i$ LSP. We then analyse in Sect. III the experimental bounds, especially on the $L_i Q_j \bar{D}_k$ operator, which restrict the $\tilde{\nu}_i$ LSP parameter space. In Sect. IV we investigate in detail the conditions at the GUT scale leading to a $\tilde{\nu}_i$ LSP. This is the central part of our work. Finally, in Sect. V, we simulate SUSY events at the LHC within one $\tilde{\nu}_\mu$ LSP scenario. We focus on signatures, which are special for $\tilde{\nu}_i$ LSP scenarios. We conclude in Sect. VI.

II. THE MODEL

The most general gauge invariant and renormalizable superpotential of the SSM is [20]

$$W_{\text{SSM}} = W_{P_6} + W_{\mathcal{P}_6}, \quad (1)$$

$$W_{P_6} = \epsilon_{ab} [(\mathbf{Y}_E)_{ij} L_i^a H_d^b \bar{E}_j + (\mathbf{Y}_D)_{ij} Q_i^{ax} H_d^b \bar{D}_{jx} + (\mathbf{Y}_U)_{ij} Q_i^{ax} H_u^b \bar{U}_{jx} + \mu H_d^a H_u^b], \quad (2)$$

$$W_{\mathcal{P}_6} = \epsilon_{ab} \left[\frac{1}{2} \lambda_{ijk} L_i^a L_j^b \bar{E}_k + \lambda'_{ijk} L_i^a Q_j^{bx} \bar{D}_{kx} \right] + \epsilon_{ab\kappa i} L_i^a H_u^b + \frac{1}{2} \epsilon_{xyz} \lambda''_{ijk} \bar{U}_i^x \bar{D}_j^y \bar{D}_k^z. \quad (3)$$

where $i, j, k = 1, 2, 3$ are generation indices. We have employed the standard notation of Ref. [21].

The superpotential, Eq. (1), consists of two different parts. The second part, $W_{\mathcal{P}_6}$, contains lepton and baryon number violating operators. If simultaneously present, they lead to rapid proton decay, in disagreement with experimental observations [8, 22, 23, 24]. An additional discrete symmetry is therefore required to keep the proton stable [4, 25].

* markus@th.physik.uni-bonn.de

† spd@th.physik.uni-bonn.de

‡ dreiner@th.physik.uni-bonn.de

§ sgrab@th.physik.uni-bonn.de

The SSM with R-parity, which prohibits $W_{\mathcal{P}_6}$, is conventionally denoted the MSSM. In a more general approach, proton-hexality, \mathcal{P}_6 , in addition prohibits dangerous dimension-five proton decay operators [4]. Here, we consider a third possibility, baryon-triality, \mathcal{B}_3 , which violates R-parity and \mathcal{P}_6 by prohibiting only the $\bar{U}\bar{D}\bar{D}$ operators in Eq. (3). R-parity, proton-hexality and baryon-triality are the only discrete gauge anomaly-free symmetries of the SSM [4, 25]. \mathcal{B}_3 models including also a dark matter candidate have been, for example, proposed in Refs. [26].

A. \mathcal{P}_6 mSUGRA Model

The MSSM with conserved \mathcal{P}_6 has 124 free parameters [27]. In the mSUGRA model with conserved \mathcal{P}_6 and radiative electroweak symmetry breaking (REWSB) [28, 29] this is reduced to five parameters, which is more manageable for phenomenological studies,

$$M_0, M_{1/2}, A_0, \tan\beta, \text{sgn}(\mu). \quad (4)$$

M_0 , $M_{1/2}$ and A_0 are the universal scalar mass, the universal gaugino mass and the universal trilinear scalar interaction at the GUT scale (M_{GUT}), respectively. $\tan\beta$ is the ratio of the vacuum expectation values of the two Higgs doublets; see Eq. (2). Finally, we choose with $\text{sgn}(\mu)$ unambiguously one solution of the electroweak symmetry breaking scalar potential ($|\mu|$ is determined by REWSB).

Using the five parameters at M_{GUT} , Eq. (4), and the RGEs to evolve the parameters down to the electroweak scale (M_Z), the mass spectrum of the sparticles and their interactions is completely determined. The left- (right-)handed charged slepton, $\tilde{\ell}_{L(R)}$, and $\tilde{\nu}$ masses of the first two generations can be approximated at M_Z by [30]:

$$\begin{aligned} m_{\tilde{\ell}_R}^2 &= M_0^2 + 0.15M_{1/2}^2 - \sin^2\theta_W M_Z^2 \cos 2\beta, \\ m_{\tilde{\ell}_L}^2 &= M_0^2 + 0.52M_{1/2}^2 - (0.5 - \sin^2\theta_W)M_Z^2 \cos 2\beta, \\ m_{\tilde{\nu}}^2 &= M_0^2 + 0.52M_{1/2}^2 + 0.5M_Z^2 \cos 2\beta, \end{aligned} \quad (5)$$

where M_Z is the Z -boson mass and θ_W is the weak-mixing angle; see also the original work of Ref. [31]. The third terms in Eq. (5) originate from the D-term quartic interactions.

For the sleptons of the third generation, the mixing between left and right chiral states is non-negligible. The stau mass matrix $\mathcal{M}_{\tilde{\tau}}$ is given by [32]

$$\mathcal{M}_{\tilde{\tau}}^2 = \begin{pmatrix} m_{\tilde{\tau}}^2 + A_{LL} & m_{\tau} B_{LR} \\ m_{\tau} B_{LR} & m_{\tilde{\tau}}^2 + C_{RR} \end{pmatrix}, \quad (6)$$

with

$$\begin{aligned} A_{LL} &= M_{\tilde{\tau}_L}^2 - (0.5 - \sin^2\theta_W)M_Z^2 \cos 2\beta, \\ B_{LR} &= A_{\tau} - \mu \tan\beta, \\ C_{RR} &= M_{\tilde{\tau}_R}^2 - \sin^2\theta_W M_Z^2 \cos 2\beta. \end{aligned} \quad (7)$$

We denote with m_{τ} the tau lepton mass and with $M_{\tilde{\tau}_L}$ and $M_{\tilde{\tau}_R}$ the left- and right-handed third generation softbreaking stau mass parameters, respectively. At M_Z , they can be approximated by [30],

$$\begin{aligned} M_{\tilde{\tau}_R}^2 &= M_0^2 + 0.15M_{1/2}^2 - \frac{2}{3}X_{\tau}, \\ M_{\tilde{\tau}_L}^2 &= M_0^2 + 0.52M_{1/2}^2 - \frac{1}{3}X_{\tau}, \\ X_{\tau} &\equiv 10^{-4}(1 + \tan^2\beta) \left(M_0^2 + 0.15M_{1/2}^2 + 0.33A_0^2 \right). \end{aligned} \quad (8)$$

Here, X_{τ} parametrizes the influence of the tau Yukawa coupling on the running of the stau masses.

An interesting property of REWSB is that over most of the parameter space one finds that $\mu^2 \gg M_Z^2$. This leads to approximate relations between neutralino and gaugino masses at M_Z . The $\tilde{\chi}_1^0$ is dominantly binolike in mSUGRA models and its mass can be approximately written as [30]

$$m_{\tilde{\chi}_1^0} \simeq M_1 = 0.41M_{1/2}, \quad (9)$$

In most of the \mathcal{P}_6 mSUGRA parameter space the $\tilde{\chi}_1^0$ or the $\tilde{\tau}_1$ is the LSP [9, 10, 31].

B. \mathcal{B}_3 mSUGRA Model

The SSM allows also for lepton number violating interactions, *cf.* Eq. (3). These additional interactions increase the number of free parameters from 124 to more than 200. For detailed phenomenological studies, the \mathcal{B}_3 mSUGRA model was proposed in Ref. [9]. Beyond the five mSUGRA parameters, Eq. (4), we assume one additional positive coupling $\Lambda' \in \{\lambda'_{ijk}\}$ at M_{GUT} [99]. We thus have the six free parameters:

$$M_0, M_{1/2}, A_0, \tan\beta, \text{sgn}(\mu), \Lambda'. \quad (10)$$

Due to the presence of one λ'_{ijk} coupling at M_{GUT} , the following changes in collider phenomenology take place compared to \mathcal{P}_6 conserving mSUGRA:

- The RGEs get additional contributions and consequently the sparticle mass spectrum and the couplings at M_Z are altered [9, 10, 33].
- The LSP can decay into SM particles via the λ'_{ijk} coupling. In principle any sparticle can now be the LSP, because the cosmological bound on stable LSPs no longer holds [6].
- Sparticles may be produced singly, possibly on resonance [15, 23, 34], *e.g.* single slepton production at hadron colliders [18, 35, 36].
- The decay patterns of the sparticles can change due to changes in the mass spectrum and the additional \mathcal{B}_3 interactions; see Refs. [10, 18] for explicit examples.

In this paper we mainly focus on the first aspect and investigate the effect of a non-vanishing $\lambda'_{ijk}|_{\text{GUT}}$ on the running of the sparticle masses. We show, that a large region in the B_3 mSUGRA parameter space exists, where a $\tilde{\nu}_i$ is the LSP. This is consistent with all present experimental constraints.

C. Sneutrino LSPs in B_3 mSUGRA

In order to understand the dependence of the $\tilde{\nu}_i$ mass at M_Z on the parameters of Eq. (10) at the GUT scale, we must take a closer look at the relevant RGEs. According to Ref. [9], the dominant contributions are [100]:

$$16\pi^2 \frac{d(m_{\tilde{\nu}_i}^2)}{dt} = -\frac{6}{5}g_1^2 M_1^2 - 6g_2^2 M_2^2 - \frac{3}{5}g_1^2 \mathcal{S} + 6\lambda_{ijk}'^2 \left[(\mathbf{m}_{\tilde{\mathbf{L}}})_{ii}^2 + (\mathbf{m}_{\tilde{\mathbf{Q}}})_{jj}^2 + (\mathbf{m}_{\tilde{\mathbf{D}}})_{kk}^2 \right] + 6(\mathbf{h}_{\tilde{\mathbf{D}}^k})_{ij}^2 \quad (11)$$

with

$$(\mathbf{h}_{\tilde{\mathbf{D}}^k})_{ij} \equiv \lambda'_{ijk} \times A_0 \quad \text{at } M_{\text{GUT}}, \quad (12)$$

and

$$\mathcal{S} \equiv \text{Tr}[\mathbf{m}_{\tilde{\mathbf{Q}}}^2 - \mathbf{m}_{\tilde{\mathbf{L}}}^2 - 2\mathbf{m}_{\tilde{\mathbf{U}}}^2 + \mathbf{m}_{\tilde{\mathbf{D}}}^2 + \mathbf{m}_{\tilde{\mathbf{E}}}^2] + m_{H_u}^2 - m_{H_d}^2. \quad (13)$$

Here g_1, g_2 are the U(1) and SU(2) gauge couplings, respectively. $t = \ln Q$ with Q the renormalization scale. $(\mathbf{h}_{\tilde{\mathbf{D}}^k})_{ij}$ is the soft breaking coupling corresponding to λ'_{ijk} . The bold-faced soft mass parameters in Eqs. (11) and (13) are 3×3 matrices in flavor space: $\mathbf{m}_{\tilde{\mathbf{Q}}}$ and $\mathbf{m}_{\tilde{\mathbf{L}}}$ for the left-handed doublet squarks and sleptons; $\mathbf{m}_{\tilde{\mathbf{U}}}$, $\mathbf{m}_{\tilde{\mathbf{D}}}$ and $\mathbf{m}_{\tilde{\mathbf{E}}}$ for the singlet up-squarks, down-squarks and sleptons, respectively. There is no summation over repeated indices in Eq. (11).

The running of $m_{\tilde{\nu}_i}$ is governed by two different sets of terms. The first three terms in Eq. (11) are proportional to the gauge couplings squared, g_1^2 and g_2^2 . We find that the sum of these three terms is negative at every scale. They therefore lead to an increase in $m_{\tilde{\nu}_i}$, going from M_{GUT} to M_Z . This effect leads to the contribution proportional to $M_{1/2}^2$ in the approximate formula, Eq. (5), for $m_{\tilde{\nu}_i}^2$. Note, that the main contributions come from the terms proportional to the gaugino masses squared, M_1^2 and M_2^2 , because \mathcal{S} in Eq. (11), which can be negative, is identical to zero at M_{GUT} for universal scalar masses. In addition the coefficients of the M_1^2 and M_2^2 terms are larger compared to the \mathcal{S} term.

The remaining contributions are proportional to $\lambda_{ijk}'^2$ and $(\mathbf{h}_{\tilde{\mathbf{D}}^k})_{ij}^2$; the latter is also proportional to $\lambda_{ijk}'^2$ at M_{GUT} , *cf.* Eq. (12). These terms are positive and will therefore reduce $m_{\tilde{\nu}_i}$, going from M_{GUT} to M_Z . They

are also new to the B_3 mSUGRA model compared to minimal mSUGRA. The influence of these new contributions on $m_{\tilde{\nu}_i}$ depends on the magnitude of λ'_{ijk} and also on the other mSUGRA parameters, Eq. (10), especially on A_0 , as we will show in Sect. IV.

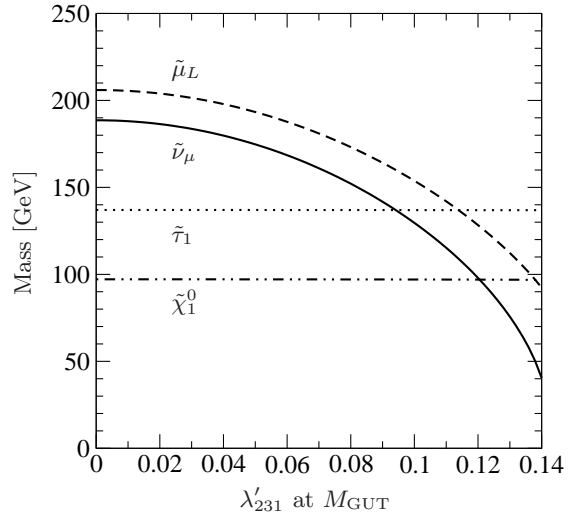


FIG. 1: Masses of $\tilde{\chi}_1^0$, $\tilde{\tau}_1$, $\tilde{\nu}_\mu$ and $\tilde{\mu}_L$ at M_Z as a function of $\lambda'_{231}|_{\text{GUT}}$. The other mSUGRA parameters are that of SPS1a [37]. We assume up-mixing, *cf.* Sect. IID.

In Fig. 1, we demonstrate the impact of a non-vanishing $\lambda'_{231}|_{\text{GUT}}$ on the running of $m_{\tilde{\nu}_i}$. We have chosen the mSUGRA point SPS1a [37], where in the P_6 conserving case, the $\tilde{\chi}_1^0$ is the LSP and the $\tilde{\tau}_1$ is the next-to-lightest supersymmetric particle (NLSP). See also Ref. [10] for the case of $\lambda'_{331}|_{\text{GUT}}$. The mass of the muon sneutrino, $\tilde{\nu}_\mu$, decreases for increasing $\lambda'_{231}|_{\text{GUT}}$, as described by Eq. (11). Furthermore, the mass of the left-handed smuon, $\tilde{\mu}_L$, decreases, as it belongs to the same SU(2) doublet. The running of the $\tilde{\mu}_L$ mass squared is also described by Eq. (11). But note that the mass difference between $\tilde{\nu}_\mu$ and $\tilde{\mu}_L$, is not the same with varying $\lambda'_{231}|_{\text{GUT}}$ as can be seen in Fig. 1. This is due to the different D-term contributions to $m_{\tilde{\nu}_\mu}$ and $m_{\tilde{\mu}_L}$, *cf.* Eq. (5), for different $\lambda'_{231}|_{\text{GUT}}$. The mass difference is approximately 20 GeV (50 GeV) for $\lambda'_{231}|_{\text{GUT}} = 0.0$ (0.14). The $\tilde{\mu}_L$ is also always heavier than the $\tilde{\nu}_\mu$, as long as $\tan\beta > 1$. We calculated the sparticle masses in Fig. 1 with an unpublished B_3 version of SOFTSUSY [38, 96].

At one-loop order, the masses of the $\tilde{\chi}_1^0$ and the $\tilde{\tau}_1$, are not changed, as can be seen in Fig. 1. They do not directly couple to the $L_2 Q_3 \bar{D}_1$ operator, in contrast to $\tilde{\nu}_\mu$, $\tilde{\mu}_L$. We therefore obtain for the parameter set SPS1a with $\lambda'_{231}|_{\text{GUT}} > 0.12$ a new candidate for the LSP, namely the sneutrino! In the following, we systematically investigate the conditions which lead to a $\tilde{\nu}_i$ LSP in B_3 mSUGRA models. From Eq. (11) it is clear that we need a coupling $\lambda'_{ijk}|_{\text{GUT}} \neq 0$. The smallest $\lambda'_{ijk}|_{\text{GUT}}$ coupling which we found leading to a $\tilde{\nu}_i$ LSP is $\lambda'_{ijk}|_{\text{GUT}} = 0.054$. Otherwise, the new con-

tributions in the RGE, Eq. (11), are not large enough to reduce $m_{\tilde{\nu}_i}$ significantly.

A non-vanishing $\lambda'_{ijk}|_{\text{GUT}}$ also reduces the left-handed squark masses of generation j and the right-handed down-squark masses of generation k , because these squarks couple directly to the $L_i Q_j \bar{D}_k$ operator [10]. One might worry that this effect leads to unwanted flavour changing neutral currents (FCNCs), when we rotate the quarks and squarks from the flavour-basis to their mass-basis. But, for example for SPS1a with $\lambda'_{231}|_{\text{GUT}} = 0.13$, the respective squark masses are reduced by less than 4%, thus avoiding FCNCs which are in contradiction with experiment [39].

We investigate in Sect. III the experimental bounds on B_3 mSUGRA models with a $\tilde{\nu}_i$ LSP. For this purpose, we need to take a closer look at quark-flavour mixing.

D. Quark Mixing

The RGEs of the different B_3 couplings are coupled via the matrix elements of the lepton- and quark-Yukawa matrices, Eq. (2). Assuming a diagonal lepton Yukawa matrix, \mathbf{Y}_E , a non-vanishing λ'_{ijk} coupling at M_{GUT} will generate at M_Z all other B_3 couplings which violate the same lepton number, see also Ref. [18]. We thus need to know the up- and down-quark Yukawa matrices, \mathbf{Y}_U and \mathbf{Y}_D , respectively.

From experiment, we only know the Cabibbo-Kobayashi-Maskawa (CKM) matrix

$$\mathbf{V}_{\text{CKM}} = \mathbf{V}_{\text{uL}} \mathbf{V}_{\text{dL}}^\dagger. \quad (14)$$

Here, \mathbf{V}_{uL} (\mathbf{V}_{dL}) rotates the left-handed up- (down-) type quarks from the electroweak basis to the mass basis. For simplicity, we assume that the Yukawa matrices \mathbf{Y}_U and \mathbf{Y}_D are real and symmetric, thus $\mathbf{V}_{\text{uL}} = \mathbf{V}_{\text{uR}}$ and $\mathbf{V}_{\text{dL}} = \mathbf{V}_{\text{dR}}$. We can imagine two extreme cases. We refer to ‘‘up-mixing’’ if

$$\mathbf{V}_{\text{uL,R}} = \mathbf{V}_{\text{CKM}}, \quad \mathbf{V}_{\text{dL,R}} = \mathbf{1}_{3 \times 3}, \quad (15)$$

at M_Z , *i.e.* the up-type Yukawa matrix \mathbf{Y}_U is non-diagonal and \mathbf{Y}_D is diagonal. In the case of ‘‘down-mixing’’, we have

$$\mathbf{V}_{\text{uL,R}} = \mathbf{1}_{3 \times 3}, \quad \mathbf{V}_{\text{dL,R}} = \mathbf{V}_{\text{CKM}}^\dagger, \quad (16)$$

at M_Z . Now, the down-type Yukawa matrix \mathbf{Y}_D is non-diagonal and \mathbf{Y}_U is diagonal. For a more detailed discussion see for example Refs. [9, 18, 40].

III. EXPERIMENTAL BOUNDS ON $\tilde{\nu}$ LSP MODELS

We have shown above that a non-vanishing coupling λ'_{ijk} at M_{GUT} can affect the spectrum at M_Z such that a $\tilde{\nu}_i$ is the LSP. This requires $\lambda'_{ijk}|_{\text{GUT}} \gtrsim 0.05$,

corresponding to $\lambda'_{ijk} \gtrsim 0.15$ at M_Z . In this section, we investigate for which couplings $\lambda'_{ijk}|_{\text{GUT}}$ the upper bounds are sufficiently weak such that a $\tilde{\nu}_i$ LSP can be generated. For the bounds, we first take into account the generation of tree level neutrino masses. Then we review other indirect bounds on these couplings. Finally we discuss the restrictions from direct searches for supersymmetric particles at LEP, at the Tevatron and the CERN $p\bar{p}$ collider.

A. Bounds from Tree Level Neutrino Masses

If $\lambda'_{ijk}|_{\text{GUT}} \neq 0$ and the bilinear coupling $\kappa_i|_{\text{GUT}} = 0$, *cf.* Eq. (3), $\kappa_i|_{M_Z} \neq 0$ will be generated via the RGEs [9, 41, 42, 43, 44]

$$16\pi^2 \frac{d\kappa_i}{dt} = -3\mu\lambda'_{ijk}(\mathbf{Y}_D)_{jk} + \dots \quad (17)$$

Furthermore, $\lambda'_{ijk}|_{\text{GUT}}$ will generate the corresponding soft breaking term of κ_i , namely \tilde{D}_i , via [9, 41, 42, 43, 44]

$$16\pi^2 \frac{d\tilde{D}_i}{dt} = -3 \left[2\mu(\mathbf{h}_{D^k})_{ij} + \tilde{B}\lambda'_{ijk} \right] (\mathbf{Y}_D)_{jk} + \dots \quad (18)$$

Here, \tilde{B} is the soft breaking coupling corresponding to μ and is determined by REWSB [9, 29]. Since the RGEs are different for κ_i and \tilde{D}_i , they are not aligned at the weak scale and can not be rotated away through a field redefinition.

The neutrino of generation i will develop a vacuum expectation value v_i due to the non-vanishing couplings κ_i and \tilde{D}_i . The vacuum expectation value v_i , and the κ_i operator will mix the neutralino fields with the neutrino fields which generates one massive neutrino, m_{ν_i} , for non-vanishing $\lambda'_{ijk}|_{\text{GUT}}$ at tree-level [9, 44, 45, 46, 47].

Demanding that this neutrino mass is smaller than the cosmological bound on the sum of neutrino masses, determined by the combination of the WMAP data [48] and the 2dFGRS data [49],

$$\sum_i m_{\nu_i} < 0.71 \text{ eV}, \quad (19)$$

results in upper bounds on $\lambda'_{ijk}|_{\text{GUT}}$, which were calculated in Ref. [9] for the parameter point SPS1a [37].

It was found in Ref. [9], assuming quark mixing solely in the down-sector (16) and assuming no accidental cancellations, that the bounds on $\lambda'_{ijk}|_{\text{GUT}}$ are of the order of $\mathcal{O}(10^{-3} - 10^{-6})$. However, if quark mixing is solely in the up-sector (15), than $(\mathbf{Y}_D)_{jk}$ vanishes at M_Z for $j \neq k$. This suppresses the right hand side of Eq. (17) and Eq. (18). The neutrino masses and therefore the bounds on $\lambda'_{ijk}|_{\text{GUT}}$ are significantly softened. Taking also two loop effects into account,

coupling	upper bounds at M_Z	LSP
λ'_{121}	$0.03 \times (m_{\tilde{c}_L}/100 \text{ GeV})$	$\tilde{\nu}_e$
λ'_{131}	$0.02 \times (m_{\tilde{t}_L}/100 \text{ GeV})$	$\tilde{\nu}_e$
λ'_{112}	$0.02 \times (m_{\tilde{s}_R}/100 \text{ GeV})$	$\tilde{\nu}_e$
λ'_{221}	$0.18 \times (m_{\tilde{s}_L}/100 \text{ GeV})$	$\tilde{\nu}_\mu$
λ'_{231}	$0.18 \times (m_{\tilde{b}_L}/100 \text{ GeV})$	$\tilde{\nu}_\mu$
λ'_{212}	$0.06 \times (m_{\tilde{s}_R}/100 \text{ GeV})$	$\tilde{\nu}_\mu$
λ'_{321}	$0.52 \times (m_{\tilde{d}_R}/100 \text{ GeV})$	$\tilde{\nu}_\tau$
λ'_{331}	$0.32 \times (m_{\tilde{d}_R}/100 \text{ GeV})$	$\tilde{\nu}_\tau$
λ'_{312}	$0.11 \times (m_{\tilde{s}_R}/100 \text{ GeV})$	$\tilde{\nu}_\tau$

TABLE I: Upper bounds on single couplings λ'_{ijk} from electroweak precision measurements. Only couplings are shown, which are consistent with the cosmological bound on neutrino masses, Eq. (19); see also Ref. [9]. The bounds depend strongly on the masses of the relevant squarks, $m_{\tilde{q}}$. The third column shows the $\tilde{\nu}_i$ LSP, which can be generated via the respective $\lambda'_{ijk|GUT}$ coupling.

we summarize in Table I the λ'_{ijk} couplings, which are unrestricted by the neutrino mass bound, Eq. (19), as long as quark mixing is dominantly in the up-sector, *cf.* Eq. (15). We also include the strictest experimental bound, which we discuss in the following subsection.

B. Indirect Bounds on λ'_{ijk}

In this section, we review the relevant indirect bounds on the couplings λ'_{ijk} from electroweak precision measurements. In Table I, we present the strongest bounds on the single λ'_{ijk} couplings at the 2σ level [8, 21, 23, 50]. The bounds apply to the couplings at M_Z . To obtain the respective bound at M_{GUT} one has to divide the corresponding bound in Table I by roughly a factor of three. For each coupling the bound depends linearly on the sfermion mass of the virtual particle exchanged in the relevant process. In the right column, we show which sneutrino can become the LSP. We see that an electron sneutrino LSP, $\tilde{\nu}_e$, is disfavoured due to the strong bounds on the couplings λ'_{ijk} . We have found that only in a small range of mSUGRA parameter space a $\tilde{\nu}_e$ LSP is found, although large squark masses weaken the bounds. In the following we will thus concentrate on muon sneutrinos, $\tilde{\nu}_\mu$, and tau sneutrinos, $\tilde{\nu}_\tau$ as LSP candidates.

One non-vanishing $\lambda'_{ijk|GUT}$ will also generate additional ($LQ\bar{D}$ and $L\bar{L}\bar{E}$) B_3 operators at M_Z , which violate the same lepton number [18]. For example, for one $\lambda'_{2jk|GUT} \neq 0$, we will generate all other muon number violating operators at M_Z via one and two loop effects. Since bounds on products of two different B_3 couplings are often much stronger than on only one B_3 coupling [8, 21, 23, 50], we have also checked that all generated products of the dominant λ'_{ijk} coupling with a generated coupling satisfy the bounds.

All products lie at least one order of magnitude below the strongest upper bounds if $\lambda'_{ijk|GUT} = 0.1$.

After REWSB, the single coupling scheme, which was assumed in deriving the bounds in Table I, cannot be realized in the quark mass eigenbasis [40]. In Sect. III A, we stated that quark mixing must be dominantly in the up-sector, Eq. (15), to fulfill the cosmological bound on the sum of neutrino masses, Eq. (19). Therefore, in the quark mass basis we will generate the following B_3 couplings

$$\tilde{\lambda}'_{imk} = (\mathbf{V}_{CKM}^*)_{mj} \lambda'_{ijk}. \quad (20)$$

$\tilde{\lambda}'_{imk}$ with $m = 1, 2, 3$ couples an up-quark superfield of generation m (in the mass basis) to a lepton and down-quark superfield of generation i and k , respectively. These effective couplings can give rise to D_0 - \bar{D}_0 mixing if $m = 1, 2$ [40, 51, 52]. D_0 oscillations were investigated by the BABAR [53, 54], Belle [55, 56] and CDF [57] collaborations. The Heavy Flavor Averaging Group combined all experimental results and obtained windows for the allowed mass difference and the allowed lifetime difference of the D_0 - \bar{D}_0 system [58].

Ref. [52] employed the experimental 2σ errors on the D_0 - \bar{D}_0 mass difference to obtain the following bounds on λ'_{ijk}

$$\begin{aligned} |\tilde{\lambda}'_{i21} \tilde{\lambda}'_{i11}| &= |\lambda_W \lambda_{i21}^{\prime 2}| \\ &\leq 0.0029 \left[\left(\frac{100 \text{ GeV}}{m_{\tilde{\ell}_{Li}}} \right)^2 + \left(\frac{100 \text{ GeV}}{m_{\tilde{d}_R}} \right)^2 \right]^{-1/2}, \end{aligned} \quad (21)$$

where $\lambda_W = 0.23$ is the Wolfenstein parameter [59] and $i = 1, 2, 3$. For the evaluation of Eq. (21), Ref. [52] assumed that the mass splitting arises solely from B_3 contributions. Note that the first equality of Eq. (21) only holds if quark mixing is solely in the up-sector, Eq. (15). The corresponding upper bound on $|\lambda_W \lambda_{i12}^{\prime 2}|$ can be obtained from Eq. (21) by replacing $m_{\tilde{d}_R}$ with $m_{\tilde{s}_R}$.

The experimentally allowed range for the difference in lifetime of the D_0 - \bar{D}_0 system was used in Ref. [51] to obtain the bounds

$$|\tilde{\lambda}'_{i21} \tilde{\lambda}'_{i11}| = |\lambda_W \lambda_{i21}^{\prime 2}| \leq 0.082 \left(\frac{m_{\tilde{\ell}_{Li}}}{100 \text{ GeV}} \right)^2. \quad (22)$$

These are valid for $i = 1, 2$. Unlike Ref. [52], Ref. [51] also took (destructive) interference between the B_3 and SM contributions into account. The bound on $|\lambda_W \lambda_{i12}^{\prime 2}|$ is the same.

If we assume a $\tilde{\ell}_{Li}$ with a mass of 200 GeV and squarks with a mass of 500 GeV, we obtain the upper bounds $\lambda'_{i21}, \lambda'_{i12} \leq 0.15$ at M_Z from the D_0 - \bar{D}_0 mass difference, Eq. (21), and $\lambda'_{i21}, \lambda'_{i12} \leq 1.2$ at M_Z from the D_0 - \bar{D}_0 lifetime difference Eq. (22). Thus the $\tilde{\nu}_i$

	$m_{\tilde{\nu}_e}$	$m_{\tilde{\nu}_\mu}$	$m_{\tilde{\nu}_\tau}$
OPAL	> 68 – 89 GeV	> 74 GeV	> 74 GeV
ALEPH	> 75 – 95 GeV	> 79 GeV	> 79 GeV

TABLE II: Lower bounds on the $\tilde{\nu}_i$ LSP masses from direct $\tilde{\nu}_i$ decay via λ'_{ijk} . The bounds were obtained from the OPAL [60] and ALEPH [61] analyses, respectively. The $\tilde{\nu}_\mu$ and $\tilde{\nu}_\tau$ mass bounds are universal. The $\tilde{\nu}_e$ mass bound depends on the chargino parameters due to potential interference effects.

LSP parameter space is strongly restricted by the D_0 – \bar{D}_0 mass difference. However it was pointed out in Ref. [51] that destructive interference, for example between P_6 violating and P_6 conserving contributions, may significantly weaken the bounds of Eq. (21), as in the case of the D_0 – \bar{D}_0 lifetime difference.

In the following, we mainly focus on the couplings λ'_{231} and λ'_{331} leading to a $\tilde{\nu}_\mu$ and $\tilde{\nu}_\tau$ LSP, respectively. These couplings are not restricted by D_0 – \bar{D}_0 mixing, because the relevant CKM matrix elements to generate $\tilde{\lambda}'_{i21}$ and $\tilde{\lambda}'_{i11}$ out of λ'_{i31} are too small, *cf.* Eq. (20).

C. Collider Constraints

1. Constraints from LEP

We now determine bounds on the $\tilde{\nu}_i$ LSP mass from LEP. For the case of a non-vanishing λ'_{ijk} coupling the $\tilde{\nu}_i$ LSP will dominantly decay into two jets:

$$\tilde{\nu}_i \rightarrow \bar{d}_j d_k. \quad (23)$$

Here, d_k (\bar{d}_j) is a (anti) down quark of generation k (j). This decay will occur instantaneously in the detector, *i.e.* with no detached vertex, since in our model λ'_{ijk} is bounded from below by the requirement of a $\tilde{\nu}_i$ LSP. $\tilde{\nu}_i$ pair production followed by the decay, Eq. (23), would lead to four jet events at LEP.

Bounds on the total $\tilde{\nu}_i$ pair production cross section, with the $\tilde{\nu}_i$ decaying via λ'_{ijk} were obtained by the OPAL collaboration [60] and also by the ALEPH collaboration [61]. From these we can obtain lower bounds on the mass of the $\tilde{\nu}_i$ LSP. We calculated the pair production cross section using the formulas given in Ref. [62], with the fine structure constant equal to its value at M_Z , *i.e.* $\alpha = 1/128$. We show in Table II the strongest lower bounds on the $\tilde{\nu}_i$ LSP masses for different lepton flavours i .

The $\tilde{\nu}_i$ LSP mass bounds for the second and third generation ($i = 2, 3$) are universal. The $\tilde{\nu}_e$ mass bound, in contrast, depends also on the chargino parameters. The chargino parameters enter through t-channel diagrams to the sneutrino pair production cross section. We calculated the different bounds on the electron sneutrino mass by assuming, that the lightest chargino

is wino-like. This is the case for most mSUGRA scenarios. We then varied its mass between 120 GeV and 1000 GeV to obtain the numbers in Table II.

In the following, we investigate the $\tilde{\nu}_\mu$ LSP and $\tilde{\nu}_\tau$ LSP parameter space in detail. A $\tilde{\nu}_e$ LSP is less favoured due to the stronger bounds on the λ'_{1jk} couplings, *cf.* Table I. We employ a lower mass bound of 78 GeV. This corresponds to the bound obtained by the ALEPH collaboration, see Table II, reduced by 1 GeV to account for numerical uncertainties in SOFTSUSY [63].

Only the mass bounds of the directly decaying $\tilde{\nu}_i$ LSP need to be considered, because all the other bounds from LEP on direct and indirect decays of heavier sparticles (compared to the $\tilde{\nu}_i$ LSP) are automatically fulfilled. In addition, the LEP exclusion bound on the light Higgs, h , is $m_h > 114.4$ GeV at 95% confidence level [66]. Anticipating a numerical error of 3 GeV of SOFTSUSYs prediction of m_h [10, 63, 64, 65], we have imposed a lower bound of 111.4 GeV.

2. Constraints from the Tevatron

At the Tevatron, a non-vanishing λ'_{ijk} coupling allows for resonant single $\tilde{\ell}_{Li}^-$ and $\tilde{\nu}_i$ production leading to dijet events

$$\bar{u}_j d_k \rightarrow \tilde{\ell}_{Li}^- \rightarrow \bar{u}_j d_k, \quad (24)$$

$$\bar{d}_j d_k \rightarrow \tilde{\nu}_i \rightarrow \bar{d}_j d_k. \quad (25)$$

The expected reach for the slepton resonance search at the Tevatron in the dijet channel is estimated in Ref. [67] as a function of the hadronic cross section for the processes in Eqs. (24), (25) and the slepton mass. In Ref. [67], the discovery potential for slepton masses between 200 GeV and 1200 GeV is given assuming an integrated luminosity of 2 fb^{-1} and 30 fb^{-1} . We have checked that all the couplings shown in Table I, assuming $\lambda'_{ijk}|_{\text{GUT}} = 0.1$, lead to production cross sections which lie at least one order of magnitude below the expected discovery region for 2 fb^{-1} given in Ref. [67]. We have employed the QCD and SUSY-QCD next-to-leading order (NLO) cross section [36].

Tevatron searches for new resonances in the dijet channel have indeed been performed by the D0 collaboration [68] and the CDF collaboration [69, 70, 71]. Although B_3 models were not considered, bounds on the production cross section of additional vector bosons, W' and Z' , which decay into two jets, were obtained. These processes are very similar to the B_3 processes, Eqs. (24) and (25). W' and Z' masses between 180 GeV and 1400 GeV were probed. In this mass region, the production cross section for a single $\tilde{\ell}_{Li}^-$ and $\tilde{\nu}_i$ with subsequent decay into two jets, lies at least one order of magnitude below the experimental limits on W' and Z' production. We assumed $\lambda'_{ijk}|_{\text{GUT}} = 0.1$ and one coupling of Table I.

process	cross section [pb]	
$P\bar{P} \rightarrow W(Z) \rightarrow q\bar{q}$	2.7×10^4	(7.9×10^3)
$P\bar{P} \rightarrow \tilde{\mu}_L \rightarrow q\bar{q}$	9.2×10^2	(5.7×10^2)
$P\bar{P} \rightarrow \tilde{\nu}_\mu \rightarrow q\bar{q}$	1.3×10^3	(8.0×10^2)

TABLE III: Hadronic cross section for dijet production via an on shell W (Z) boson in comparison to B_3 violating dijet production via $\tilde{\mu}_L$, Eq. (24) and $\tilde{\nu}_\mu$, Eq. (25), with a mass equal to the W (Z) mass. We assumed $\lambda'_{221}|_{\text{GUT}} = 0.1$. The charge conjugated processes are also taken into account.

We now estimate if the Tevatron has a chance to observe dijet pair production for $\tilde{\ell}_{Li}^-$ and $\tilde{\nu}_i$ masses *below* 180 GeV. We show in Table III the hadronic cross sections for dijet production via an on-shell W (Z) boson [72, 73]. We also give the NLO production cross section for a $\tilde{\ell}_{Li}^-$ and $\tilde{\nu}_i$ with a mass equal to the Z and W mass [36], assuming $\lambda'_{221}|_{\text{GUT}} = 0.1$. We see that the B_3 cross sections are roughly one order of magnitude smaller than the SM cross sections. We conclude that the processes, Eqs. (24) and (25), for slepton masses below 180 GeV can not be seen at the Tevatron because the Z and the W have not been observed at the Tevatron in the dijet channel so far.

Singly produced charged sleptons, Eq. (24), may also cascade decay into a lepton ℓ_i , two jets and missing energy:

$$\begin{aligned} \tilde{\ell}_{Li}^- &\rightarrow \tilde{\chi}_1^0 \ell_i^- \\ &\hookrightarrow \tilde{\nu}_i \bar{\nu}_i \\ &\hookrightarrow \bar{d}_j d_k. \end{aligned} \quad (26)$$

In principle, this signature could be more easily distinguished from the (QCD) background than pure dijet events, due to the additional isolated lepton in the final state. However the cascade decay, Eq. (26), is kinematically forbidden in most regions of the $\tilde{\nu}_i$ LSP parameter space, as we show in Sect. IV. In that case one might think about the 3-body decay, $\tilde{\ell}_{Li}^- \rightarrow \ell_i^- \bar{\nu}_i \tilde{\nu}_i$, via a virtual neutralino. However, this process can only occur at a significant rate, if the 2-body decay mode into two jets, Eq. (24), is forbidden or kinematically suppressed. This is the case for $j = 3$, *i.e.* a top quark in the final state. But the $\tilde{\ell}_{Li}^-$ can then not be produced as a single resonance, because we also need a top quark in the initial state, see Eq. (24). Furthermore the 3-body decay, $\tilde{\ell}_{Li}^- \rightarrow \ell_i^- \bar{\nu}_i \tilde{\nu}_i$, is heavily suppressed compared to the 3-body decay via a virtual top-quark, as we will see in Sect. V A.

A non-vanishing λ'_{i31} coupling can lead to B_3 top-quark decay at the Tevatron [40, 74, 75, 76, 77, 78]. For example $t \rightarrow d \tilde{\ell}_{Li}$ if $m_{\tilde{\ell}_i} < m_t$. However, the Tevatron can only test couplings λ'_{i31} via top decay, which lie at their upper bounds [78], see Table I. We use smaller λ'_{i31} couplings in the following.

A non-vanishing λ'_{i31} coupling contributes also to top-

pair production, see Refs. [78, 79, 80]. The top quarks in the $t\bar{t}$ events are polarized, since the B_3 operator couples only to left-handed top quarks. It is shown in Refs. [78, 79, 80], that the Tevatron at the end of Run II can only test couplings λ'_{i31} , which lie near their current upper bounds, *cf.* Table I. The LHC will be able to probe couplings λ'_{i31} down to $\lambda'_{i31} = 0.2$ via top polarization [80].

3. Constraints from the CERN $p\bar{p}$ Collider

Unlike D0 and CDF, the UA2 collaboration at the CERN $p\bar{p}$ collider was able to measure the hadronic decay mode of the Z and W [81]. They also searched for a W' and Z' decaying into two jets. They found no excess over the SM background and therefore set exclusion limits for W' and Z' production with masses between 80 GeV and 320 GeV [81, 82].

We compared the exclusion limits with our NLO cross section predictions for single slepton, Eq. (24), and sneutrino, Eq. (25), production assuming again $\lambda'_{ijk}|_{\text{GUT}} = 0.1$ and one of the couplings shown in Table I [36]. Our cross section prediction is at least one order of magnitude smaller than the exclusion limits in the relevant mass range.

IV. SNEUTRINO LSP PARAMETER SPACE

We have shown in Sect. II C, that one non-vanishing coupling $\lambda'_{ijk}|_{\text{GUT}} = \mathcal{O}(10^{-1})$ may lead to a $\tilde{\nu}_i$ LSP in B_3 mSUGRA models, *cf.* Fig 1. We also presented the λ'_{ijk} couplings, which have sufficiently weak upper bounds to allow for a $\tilde{\nu}_i$ LSP, see Table I. All lepton flavours are possible, although a $\tilde{\nu}_e$ LSP is disfavoured due to the stronger bounds on the λ'_{ijk} . Thus we concentrate on $\tilde{\nu}_\mu$ and $\tilde{\nu}_\tau$ LSPs in the following.

In this section, we investigate in detail the dependence of the $\tilde{\nu}_i$ LSP parameter space on the mSUGRA parameters M_0 , $M_{1/2}$, A_0 and $\tan\beta$. This is the central part of our paper. We explore 2-dimensional parameter spaces, where our scans are centered around the following points

$$\begin{aligned} \textbf{Point I: } & M_0 = 50 \text{ GeV}, M_{1/2} = 500 \text{ GeV}, \\ & A_0 = -600 \text{ GeV}, \tan\beta = 10, \\ & \text{sgn}(\mu) = +1, \lambda'_{231}|_{\text{GUT}} = 0.11, \end{aligned} \quad (27)$$

$$\begin{aligned} \textbf{Point II: } & M_0 = 200 \text{ GeV}, M_{1/2} = 290 \text{ GeV}, \\ & A_0 = -550 \text{ GeV}, \tan\beta = 12, \\ & \text{sgn}(\mu) = +1, \lambda'_{331}|_{\text{GUT}} = 0.12. \end{aligned}$$

We perform our parameter scans with an unpublished B_3 version of SOFTSUSY [38].

Point I results in a $\tilde{\nu}_\mu$ LSP with a mass of 130 GeV. The NLSP is the left-handed smuon, $\tilde{\mu}_L$, with a mass

of 159 GeV. Note that the $\tilde{\mu}_L$ mass is also reduced due to $\lambda'_{231}|_{\text{GUT}} \neq 0$, and the $\tilde{\mu}_L$ is always heavier than the $\tilde{\nu}_\mu$ for $\tan\beta > 1$, see Eq. (5) and Fig. 1. The masses of the other LSP candidates, namely the $\tilde{\tau}_1$ and the $\tilde{\chi}_1^0$, are 186 GeV and 205 GeV, respectively. Due to the rather large mass difference between the $\tilde{\nu}_\mu$ LSP on the one side, and $\tilde{\tau}_1$ and $\tilde{\chi}_1^0$ on the other, we expect an extended $\tilde{\nu}_\mu$ LSP parameter space. This is indeed the case, as shown in the following.

Point II results in a $\tilde{\nu}_\tau$ LSP with a mass of 107 GeV. The NLSP is the $\tilde{\chi}_1^0$ with a mass of 116 GeV. The NNLSP is the $\tilde{\tau}_1$, which has a large left-handed component here, because the soft breaking mass $M_{\tilde{\tau}_L}$, Eq. (8), is also reduced via the non-vanishing $\lambda'_{331}|_{\text{GUT}}$ coupling. In contrast, $M_{\tilde{\tau}_R}$ is not affected. The $\tilde{\tau}_1$ mass is 120 GeV.

The mass difference between the $\tilde{\nu}_\tau$ LSP and the $\tilde{\tau}_1$ is smaller for Point II than Point I, because $\lambda'_{331}|_{\text{GUT}}$ also reduces the mass of the $\tilde{\tau}_1$, which is an admixture of $\tilde{\tau}_L$ and $\tilde{\tau}_R$. This competes with the $\tilde{\nu}_\tau$ to be the LSP; *cf.* Ref. [10]. In contrast, $\lambda'_{231}|_{\text{GUT}} \neq 0$ reduces the mass of the $\tilde{\mu}_L$. But the $\tilde{\mu}_L$ is always heavier than the $\tilde{\nu}_\mu$. We therefore expect a smaller $\tilde{\nu}_\tau$ LSP parameter space around Point II than the $\tilde{\nu}_\mu$ LSP parameter space around Point I.

It is worth mentioning, that Point I leads to a heavier sparticle mass spectrum than Point II. This stems from the fact, that we have chosen our central scan points, such that the SUSY contributions to the anomalous magnetic moment of the muon, $\delta a_\mu^{\text{SUSY}}$, can explain the observed discrepancy, δa_μ , between experiment, a_μ^{exp} , and the SM prediction, a_μ^{SM} ,

$$\delta a_\mu = a_\mu^{\text{exp}} - a_\mu^{\text{SM}} = (29.5 \pm 8.8) \times 10^{-10}, \quad (28)$$

which corresponds to a 3.4σ deviation [83, 84, 85]. In the following, we show in our parameter scans in Figs. 4–7 contour lines, where the SUSY contributions, $\delta a_\mu^{\text{SUSY}}$, correspond to the

$$\begin{aligned} \text{central value : } \delta a_\mu^{\text{SUSY}} &= 29.5 \times 10^{-10} \\ &\Leftrightarrow \text{yellow line, labelled with "0" ,} \end{aligned}$$

$$\begin{aligned} \text{central value } \pm 1\sigma : \delta a_\mu^{\text{SUSY}} &= (29.5 \pm 8.8) \times 10^{-10} \\ &\Leftrightarrow \text{blue line, labelled with " } \pm 1 \text{ " ,} \end{aligned}$$

$$\begin{aligned} \text{central value } \pm 2\sigma : \delta a_\mu^{\text{SUSY}} &= (29.5 \pm 17.6) \times 10^{-10} \\ &\Leftrightarrow \text{green line, labelled with " } \pm 2 \text{ " ,} \end{aligned}$$

$$\begin{aligned} \text{central value } \pm 3\sigma : \delta a_\mu^{\text{SUSY}} &= (29.5 \pm 26.4) \times 10^{-10} \\ &\Leftrightarrow \text{magenta line, labelled with " } \pm 3 \text{ " .} \end{aligned} \quad (29)$$

Yellow (labelled with “0”), green (labelled with “ ± 1 ”), blue (labelled with “ ± 2 ”) and magenta (labelled with “ ± 3 ”) are the colours of the contour lines in the plots, which we show in the following sections.

The SUSY contributions to the anomalous magnetic moment of the muon, $\delta a_\mu^{\text{SUSY}}$, enter starting at the one loop level, see for example Refs. [86, 87], and involve the $\tilde{\mu}_L$ and $\tilde{\nu}_\mu$. Thus, they are enhanced if the $\tilde{\mu}_L$ and $\tilde{\nu}_\mu$ are light. As a consequence, $\delta a_\mu^{\text{SUSY}}$ increases if we switch on $\lambda'_{231}|_{\text{GUT}}$, because the mass of the $\tilde{\mu}_L$ and $\tilde{\nu}_\mu$ decrease. In contrast, $\lambda'_{331}|_{\text{GUT}}$ does not affect $\delta a_\mu^{\text{SUSY}}$. Note, that we have not included B_3 contributions to $\delta a_\mu^{\text{SUSY}}$, because they are at most at the percent level and can therefore be neglected [88].

We also consider the constraints from the $\text{BR}(b \rightarrow s\gamma)$. The current experimental value is [89]

$$\text{BR}(b \rightarrow s\gamma) = (3.52 \pm 0.25) \times 10^{-4}. \quad (30)$$

Here we have added the statistical and systematic errors in quadrature [89]. If we also include the combined theoretical error of 0.3×10^{-4} [90] we obtain the 2σ window

$$2.74 \times 10^{-4} < \text{BR}(b \rightarrow s\gamma) < 4.30 \times 10^{-4}, \quad (31)$$

where we have now added theoretical and experimental errors in quadrature.

The complete $\tilde{\nu}_\mu$ LSP parameter space, which we will show in the following, *i.e.* Figs. 4, 6(a), 7(a), is consistent with $\text{BR}(b \rightarrow s\gamma)$ at the 2σ level Eq. (31). The $\tilde{\nu}_\tau$ LSP parameter space in the A_0 - $\tan\beta$ [$M_{1/2}$ - M_0] plane, Fig. 6(b) [Fig. 7(b)] is consistent with $\text{BR}(b \rightarrow s\gamma)$ at 2σ , Eq. (31) for $\tan\beta \lesssim 11$ [$M_{1/2} \gtrsim 290$ GeV] corresponding to the dashed black line in Fig. 6(b) [Fig. 7(b)]. We will show mainly contour lines for $\delta a_\mu^{\text{SUSY}}$ in the following, *cf.* Eq. (29), because the experimental value of a_μ is in general more restrictive on the $\tilde{\nu}_i$ LSP parameter space than $\text{BR}(b \rightarrow s\gamma)$.

We finally want to point out that the complete $\tilde{\nu}_\mu$ and $\tilde{\nu}_\tau$ LSP parameter space, which we will show in the next three sections poses a branching ratio for $B_s \rightarrow \mu^+\mu^-$, which lies at least one order of magnitude below the current experimental upper bound [89],

$$\text{BR}(B_s \rightarrow \mu^+\mu^-) < 4.7 \times 10^8. \quad (32)$$

We have employed `micrOMEGAs1.3.7` [91] to calculate $\delta a_\mu^{\text{SUSY}}$, $\text{BR}(b \rightarrow s\gamma)$ and $\text{BR}(B_s \rightarrow \mu^+\mu^-)$. According to Ref. [10], B_3 contributions to $\text{BR}(b \rightarrow s\gamma)$ and $\text{BR}(B_s \rightarrow \mu^+\mu^-)$ can also be neglected for only one dominant $\lambda'_{ijk}|_{\text{GUT}}$.

A. A_0 Dependence

We have chosen two scenarios, Point I and Point II, Eq. (27), which we use as central values for 2-dimensional mSUGRA parameter scans. For both points $A_0 < 0$, with a magnitude of a few hundred GeV. We now show that this choice of A_0 enhances the negative contribution to the $\tilde{\nu}_i$ mass, which originates from a non-vanishing $\lambda'_{ijk}|_{\text{GUT}}$ coupling, *cf.* Eq. (11).

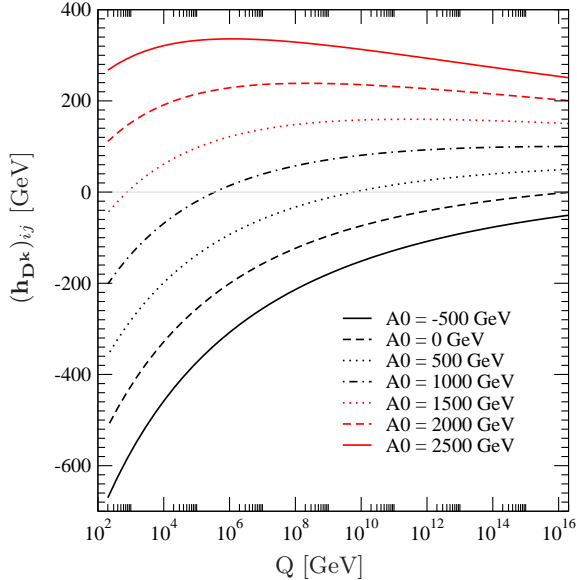


FIG. 2: Running of $(\mathbf{h}_{\mathbf{Dk}})_{ij}$ from M_{GUT} to M_Z for different values of A_0 . At M_{GUT} , we choose $M_{1/2} = 500$ GeV and $\lambda'_{ijk} = 0.1$.

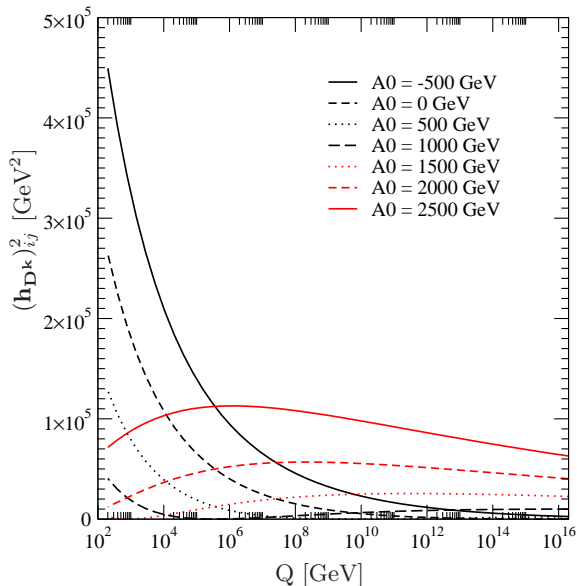


FIG. 3: Running of $(\mathbf{h}_{\mathbf{Dk}})^2_{ij}$ from M_{GUT} to M_Z for different values of A_0 . At M_{GUT} , we choose $M_{1/2} = 500$ GeV and $\lambda'_{ijk} = 0.1$.

According to Eq. (11) and (12), A_0 enters the running of $m_{\tilde{\nu}_i}$ via the B_3 soft-breaking, trilinear scalar coupling $(\mathbf{h}_{\mathbf{Dk}})_{ij}$ [9]. Thus $(\mathbf{h}_{\mathbf{Dk}})_{ij}$ gives a negative contribution to $m_{\tilde{\nu}_i}^2$, as t is decreased. It is proportional to the integral of $(\mathbf{h}_{\mathbf{Dk}})^2_{ij}$ over t , from $t_{\text{min}} = \ln(M_Z)$ to $t_{\text{max}} = \ln(M_{\text{GUT}})$.

We show in Fig. 2 the running of the trilinear scalar coupling $(\mathbf{h}_{\mathbf{Dk}})_{ij}$. We assume one non-vanishing coupling $\lambda'_{ijk}|_{\text{GUT}} = 0.1$ and a universal gaugino mass $M_{1/2} = 500$ GeV. Different lines correspond to dif-

ferent values of A_0 . We have employed the one-loop contributions from gauge interactions [9], as well as the B_3 leading interaction

$$16\pi^2 \frac{d(\mathbf{h}_{\mathbf{Dk}})_{ij}}{dt} = -(\mathbf{h}_{\mathbf{Dk}})_{ij} \left(\frac{7}{15}g_1^2 + 3g_2^2 + \frac{16}{3}g_3^2 \right) + \lambda'_{ijk} \left(\frac{14}{15}g_1^2 M_1 + 6g_2^2 M_2 + \frac{32}{3}g_3^2 M_3 \right). \quad (33)$$

M_1 , M_2 and M_3 are the U(1), SU(2) and SU(3) gaugino masses. The running of $(\mathbf{h}_{\mathbf{Dk}})_{ij}$ is dominated by the strong interaction, *i.e.* by the strong coupling g_3 and the gluino mass M_3 . The running is governed by two terms with opposite sign in Eq. (33), one proportional to λ'_{ijk} and one proportional to $(\mathbf{h}_{\mathbf{Dk}})_{ij}$.

The term proportional to λ'_{ijk} is always positive and thus decreases $(\mathbf{h}_{\mathbf{Dk}})_{ij}$ when we go from M_{GUT} to M_Z . Note, that we assume λ'_{ijk} is positive. Furthermore, the gluino mass M_3 will increase by a factor of roughly 2.5 and also λ'_{ijk} will increase by roughly a factor of 3 when we run from M_{GUT} to M_Z . Therefore this term gets relatively more important towards lower scales.

The sign of the term proportional to $(\mathbf{h}_{\mathbf{Dk}})_{ij}$ depends on the sign of A_0 , according to Eq. (12). At M_{GUT} , this term is positive (negative) for negative (positive) A_0 . Therefore, for positive A_0 , the term proportional to $(\mathbf{h}_{\mathbf{Dk}})_{ij}$ increase $(\mathbf{h}_{\mathbf{Dk}})_{ij}$ when we run from M_{GUT} to M_Z .

We can now understand the running of $(\mathbf{h}_{\mathbf{Dk}})_{ij}$ in Fig. 2. Looking at the solid red line, $A_0 = 2500$ GeV, we see that $(\mathbf{h}_{\mathbf{Dk}})_{ij}$ first increases when we go from M_{GUT} to smaller scales. Due to the large A_0 at M_{GUT} , the negative term proportional to $(\mathbf{h}_{\mathbf{Dk}})_{ij}$ dominates and increases $(\mathbf{h}_{\mathbf{Dk}})_{ij}$. Going to lower scales the positive term proportional to λ'_{ijk} grows faster and starts to dominate at $Q \approx 10^6$ GeV. From this scale on, $(\mathbf{h}_{\mathbf{Dk}})_{ij}$ decreases. In contrast, if we start with negative A_0 (solid black line), both terms give negative contributions to the running of $(\mathbf{h}_{\mathbf{Dk}})_{ij}$. Then, $(\mathbf{h}_{\mathbf{Dk}})_{ij}$ decreases with a large slope.

The resulting running of $(\mathbf{h}_{\mathbf{Dk}})^2_{ij}$ is shown in Fig. 3. Recall Eq. (11), $m_{\tilde{\nu}_i}^2$ is reduced proportional to the integral of $(\mathbf{h}_{\mathbf{Dk}})^2_{ij}$ over t . A negative value of A_0 therefore leads to a smaller $m_{\tilde{\nu}_i}$ compared to a positive value of A_0 with the same magnitude. We expect from Fig. 3, that a $\tilde{\nu}_i$ LSP in B_3 mSUGRA is preferred for negative values of A_0 with a large magnitude. We also expect, that $m_{\tilde{\nu}_i}$ in the A_0 direction has a maximum at $A_0 = 1000$ GeV, if $M_{1/2} = 500$ GeV. In general, there should be a line in the $M_{1/2}$ - A_0 plane, where $m_{\tilde{\nu}_i}$ is “maximal”, falling to either side.

We show in Fig. 4 the mass difference in GeV between the NLSP and the LSP as a function of $M_{1/2}$ and A_0 . The other mSUGRA parameters are $M_0 = 0$ GeV, $\tan\beta = 10$, $\text{sgn}(\mu) = +1$ and $\lambda'_{231}|_{\text{GUT}} = 0.16$. The yellow (labelled with “0”), blue (labelled with “ ± 1 ”)

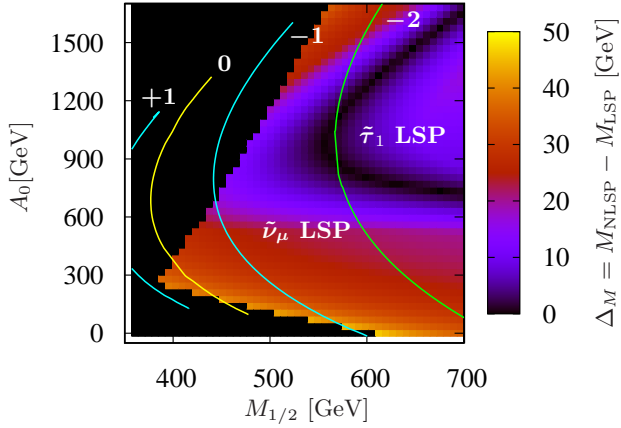


FIG. 4: Mass difference in GeV between the NLSP and the LSP as a function of $M_{1/2}$ and A_0 . The other mSUGRA parameters are $M_0 = 0$ GeV, $\tan\beta = 10$, $\text{sgn}(\mu) = +1$ and $\lambda'_{231}|_{\text{GUT}} = 0.16$. We observe a $\tilde{\nu}_\mu$ LSP and a $\tilde{\tau}_1$ LSP region. The contour lines correspond to different SUSY contributions to the anomalous magnetic moment of the muon, *cf.* Eq. (29). The blackened out region is excluded due to tachyons or the LEP $\tilde{\nu}_\mu$, h mass bounds, see Sect. III C 1.

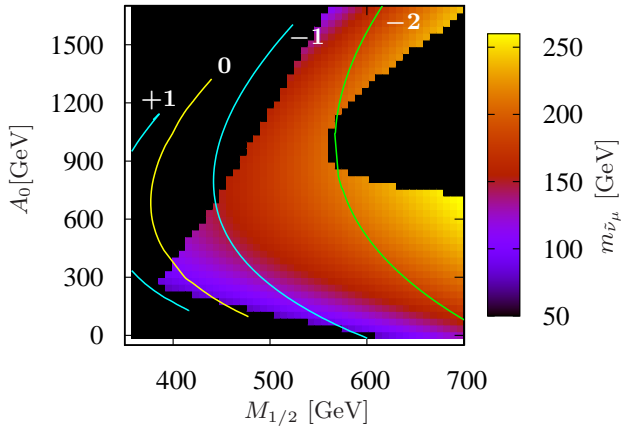


FIG. 5: Mass of the $\tilde{\nu}_\mu$ in GeV for the $\tilde{\nu}_\mu$ LSP region shown in Fig. 4.

and green (labelled with “ ± 2 ”) line indicate the SUSY contributions to the anomalous magnetic moment of the muon as described in Eq. (29). The blackened out region corresponds to mSUGRA points, which lead to tachyons or where $m_{\tilde{\nu}_\mu}$ or m_h lies below the LEP bound, see Sect. III C 1. In Fig. 5, we give the mass of the $\tilde{\nu}_\mu$ in GeV for the $\tilde{\nu}_\mu$ LSP region shown in Fig. 4.

We see in Fig. 4 a region with a $\tilde{\nu}_\mu$ LSP and a region with a $\tilde{\tau}_1$ LSP. The cross over region is marked in black. We get a $\tilde{\nu}_\mu$ LSP for small and very large values of A_0 , as expected from Fig. 3. We also see in Fig. 5 that $m_{\tilde{\nu}_\mu}$ is maximal for $M_{1/2} = 500$ GeV and $A_0 \approx 1000$ GeV in the A_0 direction. The region of negative A_0 is not shown in Figs. 4, 5, because the influence of $\lambda'_{ijk}|_{\text{GUT}}$ on $m_{\tilde{\nu}_\mu}$ is so enhanced, that we violate the

mass bound of 78 GeV or even obtain a tachyonic $\tilde{\nu}_\mu$ in large regions of $A_0 < 0$ GeV. In the following, we choose smaller values of $\lambda'_{ijk}|_{\text{GUT}}$.

B. A_0 - $\tan\beta$ Plane

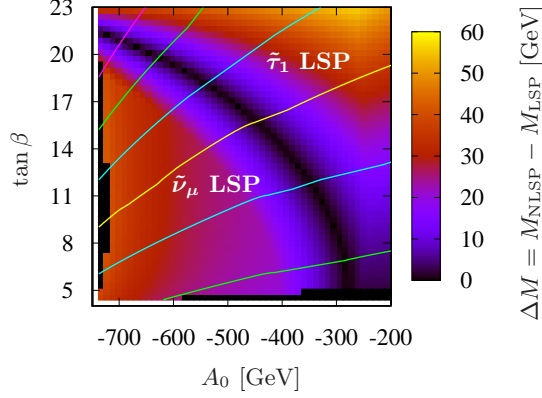
We investigate in this section the sneutrino LSP parameter space in the A_0 - $\tan\beta$ plane. As central values for our 2-dimensional scans, we choose the points given in Eq. (27).

We show in Fig. 6(a) [Fig. 6(b)] the $\tilde{\nu}_\mu$ LSP [$\tilde{\nu}_\tau$ LSP] parameter space in the A_0 - $\tan\beta$ plane. We have chosen $\lambda'_{231}|_{\text{GUT}} = 0.11$ [$\lambda'_{331}|_{\text{GUT}} = 0.12$]. Both figures show the mass difference between the NLSP and the LSP in GeV. The solid contour lines correspond to different SUSY contributions to the anomalous magnetic moment of the muon $\delta a_\mu^{\text{SUSY}}$ as described in Eq. (29). The dashed black line in Fig. 6(b) corresponds to $\text{BR}(b \rightarrow s\gamma) = 2.74 \times 10^{-4}$ (31), *i.e.* the parameter space below that line is consistent with $b \rightarrow s\gamma$ at 2σ . The blackened out region is excluded due to the presence of tachyons or by the LEP $\tilde{\nu}_\mu/\tau$ and Higgs mass bound, see Sect. III C 1.

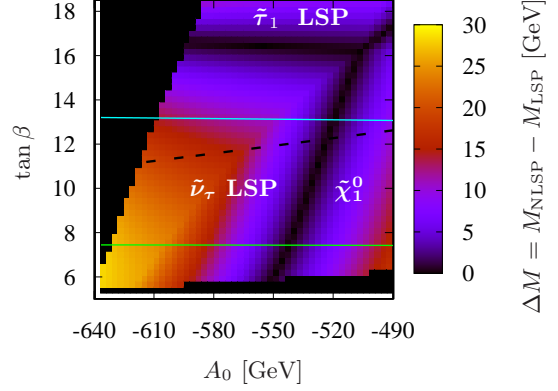
We observe that the $\tilde{\nu}_\mu$ LSP lives in an extended region of B_3 mSUGRA parameter space. For $\tan\beta = 6$, we find a $\tilde{\nu}_\mu$ LSP between $A_0 = -750$ GeV and $A_0 = -300$ GeV. For $A_0 = -700$ GeV, we find a $\tilde{\nu}_\mu$ LSP between $\tan\beta = 4$ and $\tan\beta = 21$. We also observe that most of the $\tilde{\nu}_\mu$ LSP region is consistent with the observed anomalous magnetic moment of the muon at the 1σ (blue lines) and 2σ (green lines) level, *cf.* Eq. (29). Recall, that the complete $\tilde{\nu}_\mu$ LSP region in Fig. 6(a) is also consistent with $\text{BR}(b \rightarrow s\gamma)$ at 2σ , Eq. (31). The large region of $\tilde{\nu}_\mu$ LSP parameter space is a consequence of the choice of our central scan point, *i.e.* Point I of Eq. (27). Here, the mass difference between the $\tilde{\nu}_\mu$ LSP and the $\tilde{\tau}_1$ ($\tilde{\chi}_1^0$), *i.e.* the other LSP candidates, is rather large, namely 56 GeV (75 GeV).

We see in Fig. 6(a) that we obtain a $\tilde{\tau}_1$ LSP if we increase A_0 . We explained this in the last section. A large magnitude and negative value of A_0 enhances the (negative) effect of $\lambda'_{231}|_{\text{GUT}}$ on the $\tilde{\nu}_\mu$ mass via the soft breaking trilinear coupling $(\mathbf{h}_{D1})_{23}$. The $\tilde{\tau}_1$ mass on the other hand, depends only weakly on A_0 . The dependence is via the tau Yukawa-coupling, Eq. (8), and due to left-right-mixing, Eq. (6). According to the last section, there should also be a $\tilde{\nu}_\mu$ LSP for large values of A_0 . But in this case the Higgs mass lies below the LEP bound.

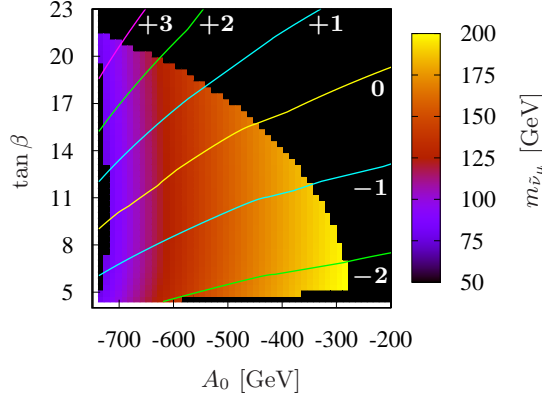
We also obtain a $\tilde{\tau}_1$ LSP, when we increase $\tan\beta$. $\tan\beta$ hardly affects the mass of the $\tilde{\nu}_\mu$ but affects the $\tilde{\tau}_1$ mass in two ways. First, increasing $\tan\beta$ increases the tau Yukawa coupling, which reduces the $\tilde{\tau}_1$ mass going from M_{GUT} to M_Z . This is parametrized by Eq. (8). Second, increasing $\tan\beta$ increases the absolute value of the off diagonal elements of the stau mass matrix,



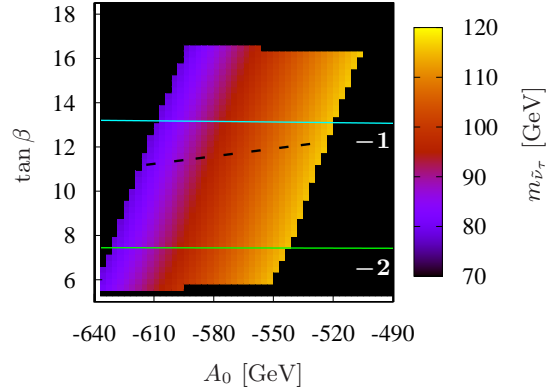
(a) Mass difference, ΔM , between the NLSP and LSP. The LSP candidates in different regions are explicitly mentioned. The blackened out region corresponds to parameter points, which possess a tachyon or where the $\tilde{\nu}_\mu$ or h mass violate the LEP bounds, Sect. III C 1.



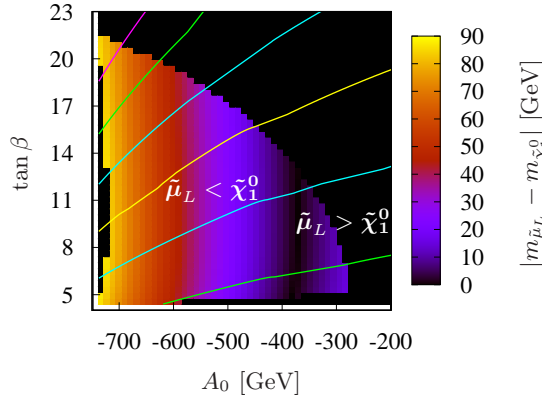
(b) Mass difference, ΔM , between the NLSP and LSP. The LSP candidates in different regions are explicitly mentioned. The blackened out region corresponds to parameter points, which possess a tachyon or where the $\tilde{\nu}_\tau$ or h mass violate the LEP bounds, cf. Sect. III C 1.



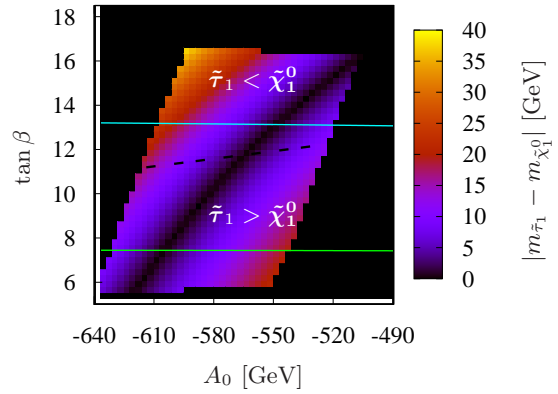
(c) $\tilde{\nu}_\mu$ mass, $m_{\tilde{\nu}_\mu}$, for the $\tilde{\nu}_\mu$ LSP region of Fig. 6(a).



(d) $\tilde{\nu}_\tau$ mass, $m_{\tilde{\nu}_\tau}$, for the $\tilde{\nu}_\tau$ LSP region of Fig. 6(b).



(e) Mass difference of the $\tilde{\mu}_L$ and $\tilde{\chi}_1^0$ for the $\tilde{\nu}_\mu$ LSP region of Fig. 6(a). We have $m_{\tilde{\mu}_L} > m_{\tilde{\chi}_1^0}$ (denoted by $\tilde{\mu}_L > \tilde{\chi}_1^0$) and $m_{\tilde{\mu}_L} < m_{\tilde{\chi}_1^0}$ (denoted by $\tilde{\mu}_L < \tilde{\chi}_1^0$).



(f) Mass difference of the $\tilde{\tau}_1$ and $\tilde{\chi}_1^0$ for the $\tilde{\nu}_\tau$ LSP region of Fig. 6(b). We have $m_{\tilde{\tau}_1} > m_{\tilde{\chi}_1^0}$ (denoted by $\tilde{\tau}_1 > \tilde{\chi}_1^0$) and $m_{\tilde{\tau}_1} < m_{\tilde{\chi}_1^0}$ (denoted by $\tilde{\tau}_1 < \tilde{\chi}_1^0$).

FIG. 6: Sneutrino LSP parameter space in the A_0 - $\tan\beta$ plane. The left panel (right panel) shows the $\tilde{\nu}_\mu$ LSP ($\tilde{\nu}_\tau$ LSP) region obtained via $\lambda_{231}|_{\text{GUT}} = 0.11$, $M_0 = 50$ GeV, $M_{1/2} = 500$ GeV and $\text{sgn}(\mu) = +1$ ($\lambda_{331}|_{\text{GUT}} = 0.12$, $M_0 = 200$ GeV, $M_{1/2} = 290$ GeV and $\text{sgn}(\mu) = +1$). The plots show from top to bottom the mass difference between the NLSP and LSP, ΔM , the mass of the sneutrino LSP, $m_{\tilde{\nu}}$, and the mass difference between the $\tilde{\chi}_1^0$ and the $\tilde{\mu}_L$ (left panel) or between the $\tilde{\chi}_1^0$ and $\tilde{\tau}_1$ (right panel). The yellow (labelled with “0”), blue (labelled with “ ± 1 ”), green (labelled with “ ± 2 ”) and magenta (labelled with “ ± 3 ”) contours correspond to different SUSY contributions to the anomalous magnetic moment of the muon, $\delta a_\mu^{\text{SUSY}}$, as described in Eq. (29). The dashed black line (right panel) corresponds to $\text{BR}(b \rightarrow s\gamma) = 2.74 \times 10^{-4}$, Eq. (31).

Eq. (6). This leads to larger left-right mixing and thus also reduces the $\tilde{\tau}_1$ mass.

Fig. 6(a) shows no region with a $\tilde{\chi}_1^0$ LSP. The entire allowed A_0 - $\tan\beta$ plane in Fig. 6(a) has a $\tilde{\tau}_1$ LSP for vanishing λ'_{231} because $M_{1/2} \gg M_0$.

We show in Fig. 6(b) the $\tilde{\nu}_\tau$ LSP parameter space. We observe a “smaller” $\tilde{\nu}_\tau$ LSP region compared to the $\tilde{\nu}_\mu$ LSP region, Fig. 6(a). We only find a $\tilde{\nu}_\tau$ LSP between $A_0 = -630$ GeV and $A_0 = -540$ GeV for $\tan\beta = 8$. In addition, the experimental 2σ windows for $\delta a_\mu^{\text{SUSY}}$, Eq. (29), and $\text{BR}(b \rightarrow s\gamma)$, Eq. (31), restrict the allowed $\tilde{\nu}_\tau$ LSP region in Fig. 6(b) to lie between $\tan\beta = 7$ and $\tan\beta = 11$.

We again obtain in Fig. 6(b) the $\tilde{\tau}_1$ as LSP when we go to larger values of $\tan\beta$ ($\tan\beta \approx 17$). Although the $\tilde{\nu}_\tau$ mass will also be reduced by a larger tau Yukawa coupling, *cf.* Eq. (8), the squared mass of the right-handed stau is reduced twice as much as the $\tilde{\nu}_\tau$ mass. In addition, $\tan\beta$ increases mixing between the $\tilde{\tau}_R$ and $\tilde{\tau}_L$, Eq. (6). But it is not possible to find a B_3 mSUGRA point, where the mass difference between the $\tilde{\nu}_\tau$ LSP and the $\tilde{\tau}_1$ is large, because $\lambda'_{331}|_{\text{GUT}}$ also reduces the mass of the $\tilde{\tau}_1$.

We also obtain in Fig. 6(b) a $\tilde{\chi}_1^0$ LSP instead of a $\tilde{\nu}_\tau$ or $\tilde{\tau}_1$ LSP if we increase A_0 beyond a certain value. The parameter space shown in Fig. 6(b) poses a $\tilde{\chi}_1^0$ LSP for vanishing $\lambda'_{331}|_{\text{GUT}}$. Increasing A_0 reduces the effect of $\lambda'_{331}|_{\text{GUT}}$ on the $\tilde{\nu}_\tau$ and $\tilde{\tau}_1$ mass, but leaves the (bino-like) $\tilde{\chi}_1^0$ mass unaffected. Thus, if the influence of $\lambda'_{331}|_{\text{GUT}}$ on the $\tilde{\nu}_\tau$ and $\tilde{\tau}_1$ mass is getting smaller, we re-obtain the $\tilde{\chi}_1^0$ as the LSP.

Finally we want to mention in our discussion of Fig. 6(b) that we have a “triple-point”, where the $\tilde{\nu}_\tau$, the $\tilde{\tau}_1$ and the $\tilde{\chi}_1^0$ are degenerate in mass. The existence of this “triple-point” is a general feature of the sneutrino LSP parameter space. This has important consequences for the LHC phenomenology, because close to a “triple-point”, we effectively have three nearly degenerate LSPs at the same time. There are also large regions in Fig. 6(a) and Fig. 6(b), where two of the three LSP candidates are nearly degenerate in mass, *i.e.* $\Delta M \leq 5$ GeV.

We present in Fig. 6(c) [Fig. 6(d)] the mass of the $\tilde{\nu}_\mu$ [$\tilde{\nu}_\tau$] for the corresponding sneutrino LSP regions of Fig. 6(a) [Fig. 6(b)]. The lightest sneutrino LSPs have a mass of 78 GeV stemming from LEP bounds, *cf.* Sect. III C 1. The heaviest sneutrino LSPs, consistent with a_μ^{exp} , Eq. (28), and $\text{BR}(b \rightarrow s\gamma)$, Eq. (31), are found in Fig. 6(c) and poses a mass of roughly 200 GeV. If one wants to have a sneutrino LSP scenario consistent with the anomalous magnetic moment of the muon, than the sneutrino mass is not allowed to be much larger than 200 GeV (see also the next section).

We show in Fig. 6(e) [Fig. 6(f)] the mass difference in GeV between the $\tilde{\chi}_1^0$ and the $\tilde{\mu}_L$ [mainly left-handed $\tilde{\tau}_1$]. Whether, $m_{\tilde{\chi}_1^0} > m_{\tilde{\mu}_L}$ [$m_{\tilde{\tau}_1}$] or $m_{\tilde{\chi}_1^0} < m_{\tilde{\mu}_L}$ [$m_{\tilde{\tau}_1}$] has important consequences for collider phenomenol-

ogy. For example, the $\tilde{\mu}_L$ can not decay into a μ and $\tilde{\chi}_1^0$ if $m_{\tilde{\chi}_1^0} > m_{\tilde{\mu}_L}$. This is the case in most of the $\tilde{\nu}_\mu$ LSP parameter space. The cascade decay, Eq. (26), is then forbidden and can not be explored at the Tevatron or LHC, as stated in Sect. III C 2. We discuss further phenomenological implications in Sect. V.

C. $M_{1/2}$ - M_0 Plane

We present in Fig. 7(a) [Fig. 7(b)] the $\tilde{\nu}_\mu$ LSP [$\tilde{\nu}_\tau$ LSP] region in the $M_{1/2}$ - M_0 plane. We have chosen $\lambda'_{231}|_{\text{GUT}} = 0.11$ [$\lambda'_{331}|_{\text{GUT}} = 0.12$]. The figures show the mass difference in GeV between the NLSP and the LSP. The solid contour lines correspond again to SUSY scenarios, which contribute to a_μ the amount described in Eq. (29) and the dashed black line in Fig. 7(b) corresponds to $\text{BR}(b \rightarrow s\gamma) = 2.74 \times 10^{-4}$ Eq. (31).

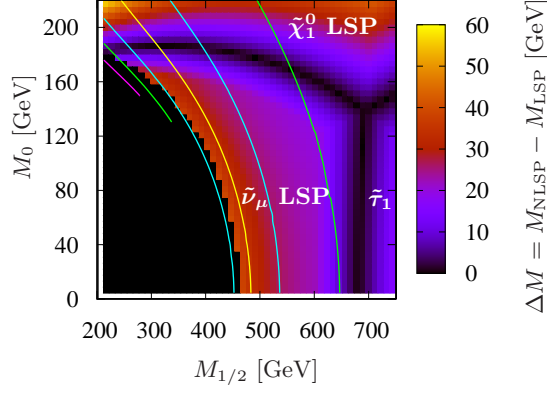
The $\tilde{\nu}_\mu$ LSP lives in an extended region of B_3 mSUGRA parameter space. This stems from the fact, that we were able to choose a central scan point, Point I of Eq. (27), where the mass difference between the $\tilde{\nu}_\mu$ LSP and the other LSP candidates, $\tilde{\tau}_1$ and $\tilde{\chi}_1^0$, is large, namely 56 GeV and 75 GeV, respectively. We find a $\tilde{\nu}_\mu$ LSP between $M_{1/2} = 350$ GeV and $M_{1/2} = 600$ GeV for $M_0 = 140$ GeV, which is consistent with a_μ^{exp} , Eq. (28), and $\text{BR}(b \rightarrow s\gamma)$, Eq. (31), at 2σ . For $M_{1/2} = 500$ GeV, we obtain a consistent $\tilde{\nu}_\mu$ LSP for $M_0 < 170$ GeV.

Nearly the entire $\tilde{\nu}_\mu$ LSP region of Fig. 7(a) is consistent with the observed value of a_μ at the 1σ (blue lines) and 2σ (green lines) level, *cf.* Eq. (29). It is also consistent with $\text{BR}(b \rightarrow s\gamma)$ at 2σ , Eq. (31).

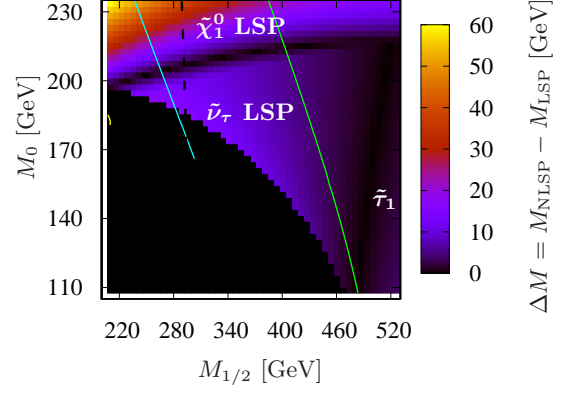
We see in Fig. 7(a), all three LSP candidates, the $\tilde{\nu}_\mu$, the $\tilde{\tau}_1$ and the $\tilde{\chi}_1^0$. If we increase M_0 , we re-obtain at $M_0 \approx 150$ GeV the $\tilde{\chi}_1^0$ LSP instead of the $\tilde{\nu}_\mu$ or the $\tilde{\tau}_1$ LSP. This is easy to understand. M_0 increases the mass of all the sfermions, see Eq. (5), but leaves the mass of the (bino-like) $\tilde{\chi}_1^0$ unaffected, *cf.* Eq. (9).

We get a $\tilde{\tau}_1$ LSP instead of a $\tilde{\nu}_\mu$ LSP for $M_{1/2} > 650$ GeV and $M_0 < 140$ GeV. Remember that the $\tilde{\tau}_1$ is mainly right-handed for non-vanishing $\lambda'_{231}|_{\text{GUT}}$ (not for large $\lambda'_{331}|_{\text{GUT}}$). According to Eq. (8), the right-handed stau mass increases more slowly with $M_{1/2}$ than the left-handed $\tilde{\nu}_\mu$ mass, Eq. (5), because the right-handed sfermions couple only to the U(1) gaugino, whereas the left-handed sfermions couple also to the SU(2) gauginos.

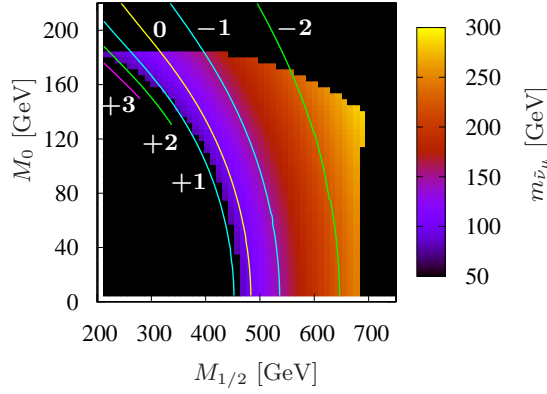
For M_0 between 140 GeV and 180 GeV, we obtain a $\tilde{\chi}_1^0$ LSP instead of a $\tilde{\nu}_\mu$ LSP if we increase $M_{1/2}$. In this region of parameter space, *i.e.* M_0 between 140 GeV and 180 GeV and $M_{1/2} < 700$ GeV, we have a $\tilde{\chi}_1^0$ LSP for vanishing $\lambda'_{231}|_{\text{GUT}}$. With $\lambda'_{231}|_{\text{GUT}} = 0.11$, we must retrieve the $\tilde{\chi}_1^0$ LSP for increasing $M_{1/2}$, because the (left-handed) $\tilde{\nu}_\mu$ couples stronger via the gauge interactions than the (bino-like) $\tilde{\chi}_1^0$; see Eq. (5) and



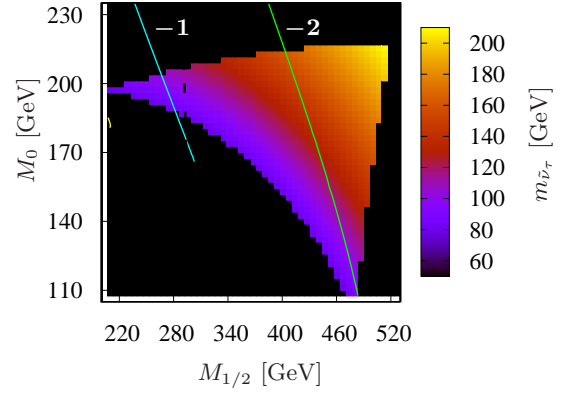
(a) Mass difference ΔM between the NLSP and LSP. The LSP candidates in different regions are explicitly mentioned. The blackened out region corresponds to parameter points, which possess a tachyon or where the $\tilde{\nu}_\mu$ or h mass violate the LEP bounds, cf. Sect. III C 1.



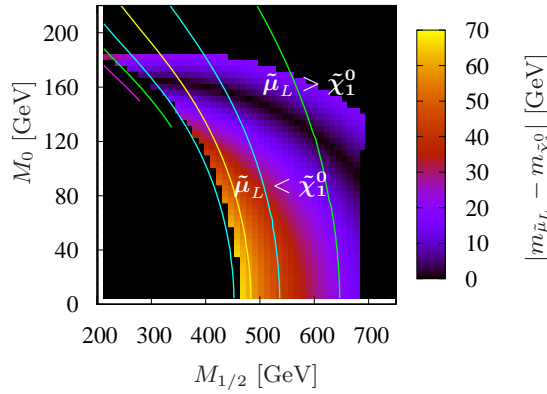
(b) Mass difference ΔM between the NLSP and LSP. The LSP candidates in different regions are explicitly mentioned. The blackened out region corresponds to parameter points, which possess a tachyon or where the $\tilde{\nu}_\tau$ or h mass violate the LEP bounds, Sect. III C 1.



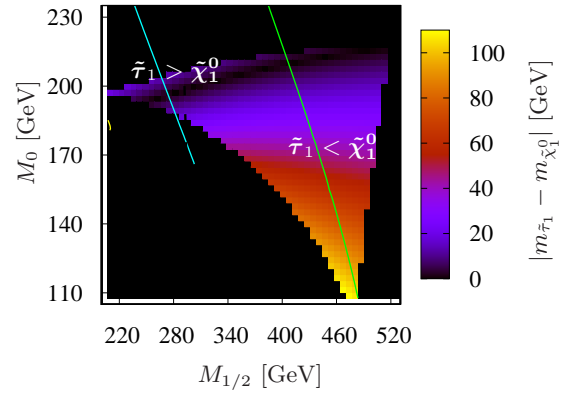
(c) $\tilde{\nu}_\mu$ mass, $m_{\tilde{\nu}_\mu}$, for the $\tilde{\nu}_\mu$ LSP region of Fig. 7(a).



(d) $\tilde{\nu}_\tau$ mass, $m_{\tilde{\nu}_\tau}$, for the $\tilde{\nu}_\tau$ LSP region of Fig. 7(b).



(e) Mass difference of the $\tilde{\mu}_L$ and $\tilde{\chi}_1^0$ for the $\tilde{\nu}_\mu$ LSP region of Fig. 7(a). We have $m_{\tilde{\mu}_L} > m_{\tilde{\chi}_1^0}$ (denoted by $\tilde{\mu}_L > \tilde{\chi}_1^0$) and $m_{\tilde{\mu}_L} < m_{\tilde{\chi}_1^0}$ (denoted by $\tilde{\mu}_L < \tilde{\chi}_1^0$).



(f) Mass difference of the $\tilde{\tau}_1$ and $\tilde{\chi}_1^0$ for the $\tilde{\nu}_\tau$ LSP region of Fig. 7(b). We have $m_{\tilde{\tau}_1} > m_{\tilde{\chi}_1^0}$ (denoted by $\tilde{\tau}_1 > \tilde{\chi}_1^0$) and $m_{\tilde{\tau}_1} < m_{\tilde{\chi}_1^0}$ (denoted by $\tilde{\tau}_1 < \tilde{\chi}_1^0$).

FIG. 7: Sneutrino LSP parameter space in the $M_{1/2}$ - M_0 plane. The left panel (right panel) shows the $\tilde{\nu}_\mu$ LSP ($\tilde{\nu}_\tau$ LSP) region obtained via $\lambda'_{231}|_{\text{GUT}}=0.11$, $A_0 = -600$ GeV, $\tan\beta = 10$ and $\text{sgn}(\mu) = +1$ ($\lambda'_{331}|_{\text{GUT}}=0.12$, $A_0 = -550$ GeV, $\tan\beta = 12$ and $\text{sgn}(\mu) = +1$). The plots show from top to bottom the mass difference between the NLSP and LSP, ΔM , the mass of the sneutrino LSP, $m_{\tilde{\nu}}$, and the mass difference between the $\tilde{\chi}_1^0$ and the $\tilde{\mu}_L$ (left panel) or between the $\tilde{\chi}_1^0$ and $\tilde{\tau}_1$ (right panel). The yellow (labelled with “0”), blue (labelled with “ ± 1 ”), green (labelled with “ ± 2 ”) and magenta (labelled with “ ± 3 ”) contours correspond to different SUSY contributions to the anomalous magnetic moment of the muon, $\delta a_\mu^{\text{SUSY}}$, as described in Eq. (29). The dashed black line in Fig. 7(b) corresponds to $\text{BR}(b \rightarrow s\gamma) = 2.74 \times 10^{-4}$, Eq. (31).

Eq. (9) respectively.

The $M_{1/2}$ - M_0 plane showing the $\tilde{\nu}_\tau$ LSP region, Fig. 7(b), looks similar to the $\tilde{\nu}_\mu$ LSP region, Fig. 7(a): We again get a $\tilde{\chi}_1^0$ LSP when we increase M_0 , and a $\tilde{\tau}_1$ LSP for larger values of $M_{1/2}$. Most of the $\tilde{\nu}_\tau$ LSP region is also consistent with the observed value of a_μ at the 1σ (blue line) or 2σ (green line) level, Eq. (29). But we must have $M_{1/2} \gtrsim 290$ GeV [dashed black line in Fig. 7(b)] to be consistent with $\text{BR}(b \rightarrow s\gamma)$ at 2σ , cf. Eq. (31). The allowed $\tilde{\nu}_\tau$ LSP region in the $M_{1/2}$ - M_0 plane is therefore “smaller” compared to the $\tilde{\nu}_\mu$ LSP region. It is worth mentioning, that one can also obtain a $\tilde{\nu}_\tau$ LSP via $\lambda'_{331}|_{\text{GUT}}$ consistent with a_μ^{exp} , Eq. (28), and $\text{BR}(b \rightarrow s\gamma)$, Eq. (31), within 1σ ; see an example in Ref. [10]. However the allowed $\tilde{\nu}_\tau$ LSP region in the $M_{1/2}$ - M_0 [A_0 - $\tan\beta$] plane is smaller in that case compared to Fig. 7(b) [Fig. 6(b)].

As explained before, $\lambda'_{331}|_{\text{GUT}}$ reduces also the mass of the $\tilde{\tau}_1$, which is also a candidate for the LSP. We can see this in Fig. 7(b) by noting that the mass difference between the $\tilde{\nu}_\tau$ LSP and the $\tilde{\tau}_1$ NLSP is rather small, *i.e.* $\Delta M \lesssim 15$ GeV. A way to increase this mass difference is to decrease $\tan\beta$; see the discussion in Sect. IV B.

Another difference between the $\tilde{\nu}_\tau$ LSP region, Fig. 7(b), and the $\tilde{\nu}_\mu$ LSP region, Fig. 7(a), is that the corresponding SUSY mass spectra for a $\tilde{\nu}_\mu$ LSP scenario are in average heavier than the SUSY mass spectra for a $\tilde{\nu}_\tau$ LSP scenario. For example, $M_0 = 100$ GeV (200 GeV) and $M_{1/2} = 500$ GeV (320 GeV) lead to squark masses of roughly 1000 GeV (700 GeV) in the $\tilde{\nu}_\mu$ LSP ($\tilde{\nu}_\tau$ LSP) parameter space. The reason is, that we have chosen our scenarios consistent with the measured value of a_μ ; see discussion after Eq. (29).

We have again in Fig. 7(a) as well as in Fig. 7(b) a “triple-point”, where the three LSP candidates are degenerate in mass.

We give in Fig. 7(c) [Fig. 7(d)] the mass of the $\tilde{\nu}_\mu$ LSP [$\tilde{\nu}_\tau$ LSP] for the sneutrino LSP region of Fig. 7(a) [Fig. 7(b)]. The sneutrino LSP masses, which lead to SUSY scenarios in agreement with a_μ^{exp} (and $b \rightarrow s\gamma$), range from 78 GeV (LEP bound, Sect. III C 1) up to roughly 250 GeV. Relaxing this bound, we claim that a_μ^{exp} puts an upper bound of roughly 300 GeV at the 2σ level on the mass of a sneutrino LSP within B_3 mSUGRA. Note that $\text{BR}(b \rightarrow s\gamma)$ increases if we increase $M_{1/2}$, whereas $\delta a_\mu^{\text{SUSY}}$ decreases, *cf.* for example Fig. 4 and Fig. 5 in Ref. [10]. The upper bound on the sneutrino LSP mass is thus due to a_μ^{exp} .

We finally show in Fig. 7(e) [Fig. 7(f)] the mass difference in GeV between the $\tilde{\chi}_1^0$ and the μ_L [mainly left-handed $\tilde{\tau}_1$]. We again observe that the $\tilde{\chi}_1^0$ is heavier than the $\tilde{\mu}_L$ in most regions of the $\tilde{\nu}_\mu$ LSP parameter space. The cascade decay, Eq. (26), is therefore not observable at the Tevatron. Further phenomenological consequences at hadron colliders will be discussed in Sect. V.

D. Sneutrino LSPs with $\lambda'_{ijk}|_{\text{GUT}} \neq \lambda'_{231}$ or λ'_{331}

We investigated in the last three sections in detail the $\tilde{\nu}_\mu$ LSP ($\tilde{\nu}_\tau$ LSP) parameter space with $\lambda'_{231}|_{\text{GUT}} = 0.11$ ($\lambda'_{331}|_{\text{GUT}} = 0.12$). We briefly consider the other couplings of Table I.

For $\lambda'_{131}|_{\text{GUT}}$, we obtain nearly the same parameter space as in Fig. 6(a) and Fig. 7(a), where $\lambda'_{231}|_{\text{GUT}} = 0.11$. We now have a $\tilde{\nu}_e$ LSP instead of a $\tilde{\nu}_\mu$ LSP. Also the mass of the left-handed selectron, \tilde{e}_L , (for $\lambda'_{131}|_{\text{GUT}} = 0.11$) equals the mass of the $\tilde{\mu}_L$ (for $\lambda'_{231}|_{\text{GUT}} = 0.11$) and vice versa. But note, that the $\tilde{\nu}_e$ LSP parameter space is much more restricted than the $\tilde{\nu}_\mu$ LSP parameter space due to the stronger bounds on λ'_{131} , *cf.* Table I. Also the LEP bound on $m_{\tilde{\nu}_e}$ is more model dependent, see Table II.

We also obtain a $\tilde{\nu}_\mu$ LSP scenario via $\lambda'_{221}|_{\text{GUT}}$ and $\lambda'_{212}|_{\text{GUT}}$. If we choose $\lambda'_{221}|_{\text{GUT}}$ or $\lambda'_{212}|_{\text{GUT}} = 0.097$, we find similar regions to Fig. 6(a) and Fig. 7(a), where the $\tilde{\nu}_\mu$ is the LSP. The effect of $\lambda'_{221}|_{\text{GUT}}$ and $\lambda'_{212}|_{\text{GUT}}$ on $m_{\tilde{\nu}_\mu}$ is stronger, because the running of both couplings involves no loops containing the large top Yukawa coupling. In contrast, the top Yukawa coupling weakens the running of λ'_{231} ($j=3!$) when we go from M_{GUT} to M_Z [9, 18].

Analogously, similar to Fig. 6(b) and Fig. 7(b), we find parameter regions, where the $\tilde{\nu}_\tau$ is the LSP. We now have to choose $\lambda'_{321}|_{\text{GUT}}$ or $\lambda'_{312}|_{\text{GUT}} = 0.104$ instead of $\lambda'_{331}|_{\text{GUT}} = 0.12$.

Note however, that different couplings λ'_{ijk} lead to a different collider phenomenology, because the $L_i Q_j \bar{D}_k$ operator couples to different generations of lepton and quark superfields. We discuss this topic in the next section.

V. HADRON COLLIDER PHENOMENOLOGY

We have shown in the last section, that a sneutrino LSP exists in an extended region of B_3 mSUGRA parameter space. We now investigate the corresponding phenomenology at hadron colliders, especially at the LHC. The main phenomenological differences between a P_6 mSUGRA scenario with a stable $\tilde{\chi}_1^0$ LSP and a B_3 mSUGRA scenario with an unstable sneutrino LSP are:

- The mass spectrum is changed. We now have a sneutrino LSP. Also some of the sleptons might be lighter than the $\tilde{\chi}_1^0$, for example the $\tilde{\mu}_L$ in the presence of $\lambda'_{231}|_{\text{GUT}}$; see Figs. 6(e), 7(e). Thus the decay chains and final state topologies are different.
- The LSP is not stable anymore and directly decays to SM particles via the B_3 coupling. In the following analysis, with $\lambda'_{231}|_{\text{GUT}} \neq 0$, we have

two extra jets from each $\tilde{\nu}_\mu$ LSP decay. This also results in less missing transverse momentum, \cancel{p}_T .

- We have shown, that $\lambda'_{ijk}|_{\text{GUT}} = \mathcal{O}(10^{-1})$ is needed to obtain a $\tilde{\nu}_i$ LSP. This large coupling can lead to direct and dominating B_3 decays of heavy sparticles; namely of left-handed charged sleptons of generation i , of left-handed squarks of generation j and of right-handed down-type squarks of generation k . The SM decay products naturally have large momenta.

In the following, we investigate these aspects in detail. We perform a Monte Carlo simulation at the parton level using the HERWIG event generator [92, 93].

A. Example Spectrum and Branching Ratios

To investigate the sneutrino LSP phenomenology at the LHC, we choose as an example a scenario with a $\tilde{\nu}_\mu$ LSP:

$$\lambda'_{231}|_{\text{GUT}} = 0.11, \quad M_0 = 100 \text{ GeV}, \quad M_{1/2} = 450 \text{ GeV}, \\ A_0 = -600 \text{ GeV}, \quad \tan\beta = 10, \quad \text{sgn}(\mu) = +1. \quad (34)$$

This benchmark point can be found in Fig. 7(a) and is consistent with a_μ^{exp} , Eq. (28), and $\text{BR}(b \rightarrow s\gamma)$, Eq. (31), at 1σ . See also Ref. [10] for a benchmark scenario with a $\tilde{\nu}_\tau$ LSP.

The resulting sparticle masses and branching ratios (BRs) are given in Table IV. The B_3 decays are shown in bold-face. Sparticle masses which are significantly affected by $\lambda'_{231}|_{\text{GUT}}$ are also bold-face. We calculate the decay rates by piping the output of SOFTSUSY through ISAWIG1.200. This is linked to ISAJET7.75 [94] in order to calculate the decay widths of the SUSY particles. This output is later fed into HERWIG to simulate events at the LHC.

We find that the decay of the $\tilde{\nu}_\mu$ LSP with a mass of 124 GeV is completely dominated by the λ'_{231} coupling. Each LSP decay leads to a bottom and a down quark and no \cancel{p}_T [97, 98]. However, \cancel{p}_T can be obtained from cascade decays of heavy sparticles. In principle, reconstruction of the $\tilde{\nu}_\mu$ mass should be possible, although combinatorial backgrounds might complicate this task.

The $\tilde{\mu}_L$ with a mass of 147 GeV is the NLSP. This is the case in most of the $\tilde{\nu}_\mu$ LSP parameter space, *cf.* Figs. 6(e), 7(e). The $\tilde{\mu}_L$ decays mainly via the $L_2 Q_3 \bar{D}_1$ operator into SM fermions, in principle to $\bar{t}d$. If this decay mode is not kinematically allowed, like for the benchmark point under study, we obtain a dominant 3-body decay into $W^- \bar{b}d$ [18]. We thus have at least two jets, where one of the jets is a b -jet. As mentioned in Sect. III C 2, another possible 3-body decay is $\tilde{\mu}_L^- \rightarrow \mu^- \bar{\nu}_\mu \tilde{\nu}_\mu$ via a virtual neutralino. But this decay is suppressed by four orders of magnitude compared to the 3-body decay via a virtual top quark. The reasons

are: small couplings (left-handed sleptons couple to a bino-like $\tilde{\chi}_1^0$), less phase space ($m_{\tilde{\mu}_L} - m_{\tilde{\nu}_\mu} = 23$ GeV), destructive interferences between diagrams with a virtual $\tilde{\chi}_1^0$ and $\tilde{\chi}_2^0$, and the decay via the virtual top is enhanced by a colour factor of 3 [18]. However, there is an additional 2-body decay mode, $\tilde{\mu}_L \rightarrow \bar{c}d$, in Table IV. This decay proceeds via a non-vanishing λ'_{221} coupling, which is generated out of $\lambda'_{231}|_{\text{GUT}}$ via RGE running [9, 18, 41].

The electroweak gauginos decay dominantly via P_6 conserving gauge interactions to 2-body final states. The lightest gaugino is the $\tilde{\chi}_1^0$, which is only the NNLSP within our benchmark scenario; $m_{\tilde{\chi}_1^0} = 184$ GeV. It decays into either the LSP or NLSP. These then undergo direct B_3 decays, as discussed before. So, the $\tilde{\chi}_1^0$ decays lead to dijet events with \cancel{p}_T or a muon. Due to the Majorana nature of the $\tilde{\chi}_1^0$, negatively and positively charged muons are possible. Cascade decays of pair produced sparticles can therefore lead to like sign-muon events via $\tilde{\chi}_1^0$ decays; see Sect. V B. Note, that $\tilde{\nu}_\mu$ LSP scenarios exist where the $\tilde{\chi}_1^0$ is also heavier than the $\tilde{\tau}_1$ or even the right-handed smuon, $\tilde{\mu}_R$, and selectron, \tilde{e}_R . These scenarios can lead to multi-lepton final states. We will not consider these scenarios here, because the relevant $\tilde{\mu}_R$ and \tilde{e}_R decays into the $\tilde{\nu}_\mu$ LSP and the $\tilde{\mu}_L$ NLSP are not implemented in HERWIG.

The $\tilde{\chi}_2^0$ also has a significant BR to $\tilde{\mu}_L^\pm \mu^\mp$ and $\tilde{\nu}_\mu \nu_\mu$. Similarly, the lightest chargino, $\tilde{\chi}_1^\pm$, decays either predominantly into $\tilde{\nu}_\mu^* \mu^\mp$ or $\tilde{\mu}_L^\pm \nu_\mu$, leading to either a muon or missing energy in the final state. The $\tilde{\chi}_2^0$ and $\tilde{\chi}_1^\pm$ are wino-like in mSUGRA models. They thus decay predominantly to the left-handed $\tilde{\mu}_L$ and $\tilde{\nu}_\mu$. The decays of the heavier chargino, $\tilde{\chi}_2^\pm$, and neutralinos, $\tilde{\chi}_{3/4}^0$ are similar to P_6 mSUGRA scenarios.

The $\tilde{\tau}_1$ in Table IV is the next-to-NNLSP (NNNLSP) with a mass of 188 GeV and almost degenerate with the $\tilde{\chi}_1^0$. The $\tilde{\tau}_1$ can in general be the NLSP, the NNLSP or NNNLSP in B_3 mSUGRA scenarios with a sneutrino LSP. Here we have $\tilde{\tau}_1^- \rightarrow \tilde{\chi}_1^0 \tau^-$.

The $\tilde{\mu}_R$, \tilde{e}_R , \tilde{e}_L , $\tilde{\nu}_e$, $\tilde{\nu}_\tau$ and $\tilde{\tau}_2$ in Table IV decay into the $\tilde{\chi}_1^0$ or, in the case of the $\tilde{\tau}_2$ and $\tilde{\nu}_\tau$, also into the $\tilde{\tau}_1$ similar to P_6 mSUGRA scenarios. But as mentioned above, the $\tilde{\tau}_1$, the $\tilde{\mu}_R$ and the \tilde{e}_R can in general be lighter than the $\tilde{\chi}_1^0$ in $\tilde{\nu}_\mu$ LSP scenarios. These particles then decay preferentially into the $\tilde{\nu}_\mu$ LSP via a 3-body decay.

The masses of the top-squarks, $\tilde{t}_{1,2}$, and the bottom-squarks, $\tilde{b}_{1,2}$, are slightly reduced due to the presence of λ'_{231} in the corresponding RGEs. The \tilde{t}_1 is the lightest squark with a mass of 650 GeV and has four 2-body decay modes with appreciable BRs. Three decays are via gauge interactions and one via λ'_{231} . Since the electroweak gauge couplings and λ'_{231} have the same order of magnitude, we also expect P_6 conserving and violating decays at a similar rate. The situation for the \tilde{t}_2 , \tilde{b}_1 and \tilde{b}_2 is similar to \tilde{t}_1 . All of these particles couple via their left-handed component to the $L_2 Q_3 \bar{D}_1$ operator

	mass [GeV]	channel	BR	channel	BR
$\tilde{\nu}_\mu$	124	$\bar{b}d$	100%		
$\tilde{\mu}_L^-$	147	$W^- \bar{b}d$	79.0%	$\bar{c}d$	21.0%
$\tilde{\chi}_1^0$	184	$\tilde{\nu}_\mu^* \nu_\mu$	36.0%	$\tilde{\nu}_\mu \bar{\nu}_\mu$	36.0%
		$\tilde{\mu}_L^+ \mu^-$	14.0%	$\tilde{\mu}_L^- \mu^+$	14.0%
$\tilde{\tau}_1^-$	188	$\tilde{\chi}_1^0 \tau^-$	100%		
$\tilde{e}_R^- (\tilde{\mu}_R^-)$	206	$\tilde{\chi}_1^0 e^- (\mu^-)$	100%		
$\tilde{\nu}_\tau$	316	$\tilde{\chi}_1^0 \nu_\tau$	67.3%	$W^+ \tilde{\tau}_1^-$	32.7%
$\tilde{\nu}_e$	319	$\tilde{\chi}_1^0 \nu_e$	100%		
\tilde{e}_L^-	329	$\tilde{\chi}_1^0 e^-$	100%		
$\tilde{\tau}_2^-$	329	$\tilde{\chi}_1^0 \tau^-$	65.1%	$h^0 \tilde{\tau}_1^-$	18.2%
		$Z^0 \tilde{\tau}_1^-$	16.7%		
$\tilde{\chi}_2^0$	350	$\tilde{\nu}_\mu \bar{\nu}_\mu$	23.7%	$\tilde{\nu}_\mu^* \nu_\mu$	23.7%
		$\tilde{\mu}_L^- \mu^+$	22.4%	$\tilde{\mu}_L^+ \mu^-$	22.4%
		$\tilde{\nu}_\tau \bar{\nu}_\tau$	1.1%	$\tilde{\nu}_\tau^* \nu_\tau$	1.1%
$\tilde{\chi}_1^-$	350	$\tilde{\nu}_\mu^* \mu^-$	49.7%	$\tilde{\mu}_L^- \bar{\nu}_\mu$	42.6%
		$\tilde{\nu}_\tau^* \tau^-$	2.3%	$\tilde{\nu}_e^* e^-$	1.8%
		$\tilde{\tau}_1^- \bar{\nu}_\tau$	1.6%		
$\tilde{\chi}_3^0$	691	$\tilde{\chi}_1^- W^+$	29.7%	$\tilde{\chi}_1^+ W^-$	29.7%
		$\tilde{\chi}_2^0 Z^0$	26.1%	$\tilde{\chi}_1^0 Z^0$	8.3%
		$\tilde{\chi}_1^0 h^0$	1.7%	$\tilde{\chi}_2^0 h^0$	1.7%
\tilde{t}_1	650	$\tilde{\chi}_1^+ b$	42.1%	$\tilde{\chi}_1^0 t$	33.5%
		$\tilde{\chi}_2^0 t$	13.8%	$\mu^+ d$	10.6%
$\tilde{\chi}_2^-$	702	$\tilde{\chi}_2^0 W^-$	28.0%	$\tilde{\chi}_1^- Z^0$	26.6%
		$\tilde{\chi}_1^- h^0$	23.8%	$\tilde{\chi}_1^0 W^-$	7.9%
		$\tilde{t}_1^* b$	4.1%	$\tilde{\mu}_L^- \bar{\nu}_\mu$	2.5%
		$\tilde{\tau}_2^- \bar{\nu}_\tau$	2.0%	$\tilde{e}_L^- \bar{\nu}_e$	1.7%
		$\tilde{\nu}_\tau^* \tau^-$	1.3%		
$\tilde{\chi}_4^0$	702	$\tilde{\chi}_1^- W^+$	28.3%	$\tilde{\chi}_1^+ W^-$	28.3%
		$\tilde{\chi}_2^0 h^0$	22.3%	$\tilde{\chi}_1^0 h^0$	7.0%
		$\tilde{\chi}_2^0 Z^0$	2.0%	$\tilde{\chi}_1^0 Z^0$	1.8%
		$\tilde{\nu}_\mu \bar{\nu}_\mu$	1.2%	$\tilde{\nu}_\mu^* \nu_\mu$	1.2%

	mass [GeV]	channel	BR	channel	BR
\tilde{b}_1	842	$W^- \tilde{t}_1$	35.8%	$\tilde{\chi}_1^- t$	31.3%
		$\tilde{\chi}_2^0 b$	18.8%	$\tilde{\nu}_\mu d$	12.4%
		$\tilde{\chi}_1^0 b$	1.2%		
\tilde{d}_R	897	$\nu_\mu b$	45.3%	$\mu^- t$	42.1%
		$\tilde{\chi}_1^0 d$	12.6%		
\tilde{t}_2	906	$Z^0 \tilde{t}_1$	28.2%	$\tilde{\chi}_1^+ b$	23.7%
		$h^0 \tilde{t}_1$	11.7%	$\tilde{\chi}_2^0 t$	10.2%
		$\mu^+ d$	9.0%	$\tilde{\chi}_4^0 t$	7.5%
		$\tilde{\chi}_2^+ b$	5.4%	$\tilde{\chi}_1^0 t$	2.6%
		$\tilde{\chi}_3^0 t$	1.7%		
\tilde{b}_2	919	$\tilde{\chi}_1^0 b$	41.3%	$W^- \tilde{t}_1$	25.3%
		$\tilde{\chi}_2^- t$	14.4%	$\tilde{\chi}_4^0 b$	5.3%
		$\tilde{\chi}_3^0 b$	5.0%	$\tilde{\nu}_\mu d$	3.4%
		$\tilde{\chi}_1^- t$	3.2%	$\tilde{\chi}_2^0 b$	1.9%
\tilde{s}_R	928	$\tilde{\chi}_1^0 s$	99.8%		
$\tilde{u}_R (\tilde{c}_R)$	932	$\tilde{\chi}_1^0 u(c)$	99.8%		
$\tilde{u}_L (\tilde{c}_L)$	963	$\tilde{\chi}_1^+ d(s)$	65.6%	$\tilde{\chi}_2^0 u(c)$	32.6%
		$\tilde{\chi}_1^0 u(c)$	1.2%		
$\tilde{d}_L (\tilde{s}_L)$	966	$\tilde{\chi}_1^- u(c)$	64.5%	$\tilde{\chi}_2^0 d(s)$	32.5%
		$\tilde{\chi}_1^0 d(s)$	1.6%	$\tilde{\chi}_2^- u(c)$	1.0%
\tilde{g}	1046	$\tilde{t}_1 \bar{t}$	15.0%	$\tilde{t}_1^* t$	15.0%
		$\tilde{b}_1 \bar{b}$	9.2%	$\tilde{b}_1^* b$	9.2%
		$\tilde{d}_R \bar{d}$	5.2%	$\tilde{d}_R^* d$	5.2%
		$\tilde{b}_2 \bar{b}$	3.9%	$\tilde{b}_2^* b$	3.9%
		$\tilde{s}_R \bar{s}$	3.4%	$\tilde{s}_R^* s$	3.4%
		$\tilde{u}_R \bar{u} (\tilde{c}_R \bar{c})$	3.2%	$\tilde{u}_R^* u (\tilde{c}_R^* c)$	3.2%
		$\tilde{u}_L \bar{u} (\tilde{c}_L \bar{c})$	1.7%	$\tilde{u}_L^* u (\tilde{c}_L^* c)$	1.7%
		$\tilde{d}_L \bar{d} (\tilde{s}_L \bar{s})$	1.6%	$\tilde{d}_L^* d (\tilde{s}_L^* s)$	1.6%

TABLE IV: Branching ratios (BRs) and sparticle masses for the example scenario defined in Eq. (34). BRs smaller than 1% are neglected. B_3 decays are shown in bold-face. Masses which are reduced by more than 5 GeV (compared to the P_6 spectrum) due to $\lambda'_{231}|_{\text{GUT}} = 0.11$ are also shown in bold-face.

and can therefore decay into two SM particles.

The masses of the left-handed and right-handed squarks of the 1st and 2nd generation are around 900 GeV. The right-handed down-squark ($m_{\tilde{d}_R} = 897$ GeV) is lighter than the right-handed strange-squark ($m_{\tilde{s}_R} = 928$ GeV). In contrast both squarks are degenerate in mass in P_6 mSUGRA. However, they are so heavy, that no problems should occur with flavour changing neutral currents. $\lambda'_{231}|_{\text{GUT}}$ couples only to the right-handed down squarks and not to the right-handed strange squarks. So, $m_{\tilde{d}_R}$ is reduced, keeping $m_{\tilde{s}_R}$ unchanged. For the same reason, there exist no B_3 decays of \tilde{s}_R via λ'_{231} at tree-level. In contrast, \tilde{d}_R has dominant direct B_3 decays to SM particles, which than have large momenta, see Sect. VB.

The heaviest sparticle is the gluino, \tilde{g} , with a mass

of 1046 GeV. It decays only via the strong interaction. The allowed decay modes and their relative BRs depend upon the sum of the final state masses. For example, $\tilde{g} \rightarrow \tilde{t}_1 t$ has the largest BR, since the \tilde{t}_1 is the lightest squark.

We conclude that the heavy part of the mass spectrum looks very similar to P_6 mSUGRA scenarios with a stable $\tilde{\chi}_1^0$ LSP. However, a non-vanishing λ'_{ijk} coupling, which has the same order of magnitude as the gauge couplings, allows for additional 2-body B_3 decays of some of the squarks. Which squarks are allowed to decay via λ'_{ijk} depend on the indices j, k . The masses and compositions of the electroweak gauginos are also very similar to P_6 mSUGRA. However, the $\tilde{\chi}_1^0$ is no longer the LSP. Depending on the specific $\tilde{\nu}_i$ LSP scenario, the $\tilde{\chi}_1^0$ can decay into charged sleptons and sneutrinos of different generations. Therefore, the

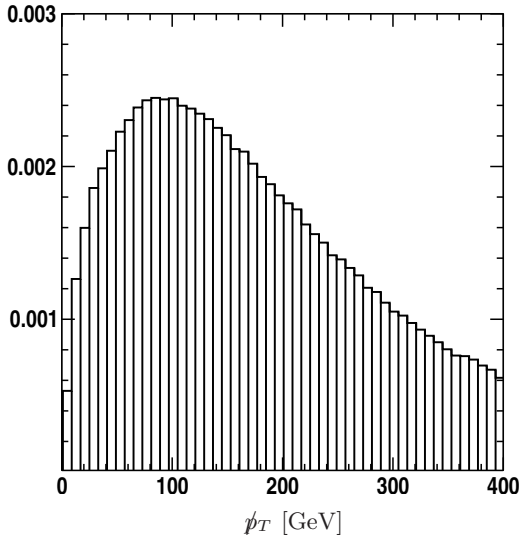


FIG. 8: \not{p}_T distribution due to neutrinos in the final state for the example scenario Eq. (34). The distribution is normalized to one. Note that events with no \not{p}_T in the final state are not shown.

main difference can be found in the light part of the mass spectrum where we have the $\tilde{\nu}_i$ LSP. The $\tilde{\nu}_i$ LSP decays preferentially into two jets via λ'_{ijk} .

B. Sparticle Pair Production

We have investigated in the last section the mass spectrum and the BRs of SUSY particles for one representative B_3 mSUGRA scenario with a $\tilde{\nu}_\mu$ LSP, described by Eq. (34). We have pointed out the general differences compared to mSUGRA scenarios with a stable $\tilde{\chi}_1^0$ LSP. We now explore signatures at the LHC which arise from pair production of sparticles via the gauge interactions, *i.e.* mainly squark and gluino production via the strong interaction. For this purpose we use the HERWIG event generator. We investigate single sparticle production in Sect. V C.

The masses of the strongly interacting sparticles are roughly 1 TeV. We therefore obtain from HERWIG a total sparticle pair production (leading order) cross section at the LHC of

$$\sigma_{\text{total}} = 3.0 \text{ pb}. \quad (35)$$

So, one can expect approximately 300 000 SUSY pair production events for an integrated luminosity of 100 fb^{-1} . The sparticle decays follow those in Table IV. The different decay chains lead to different final states. Moreover, the p_T distributions of the final state particles and the \not{p}_T can be very distinctive compared to P_6 mSUGRA with a stable $\tilde{\chi}_1^0$ LSP.

We show in Fig. 8 the \not{p}_T distribution due to neutrinos in the final state. Note, that here roughly 20% of all SUSY events possess no \not{p}_T in contrast to P_6 mSUGRA

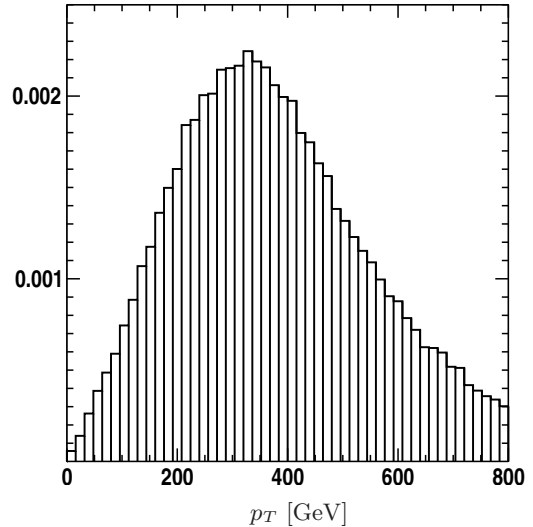


FIG. 9: p_T distribution of the muon from the decays $\tilde{d}_R \rightarrow \mu t$ and $\tilde{t}_{1/2} \rightarrow \mu d$ (*cf.* Table IV) at the LHC. The distribution is normalized to one.

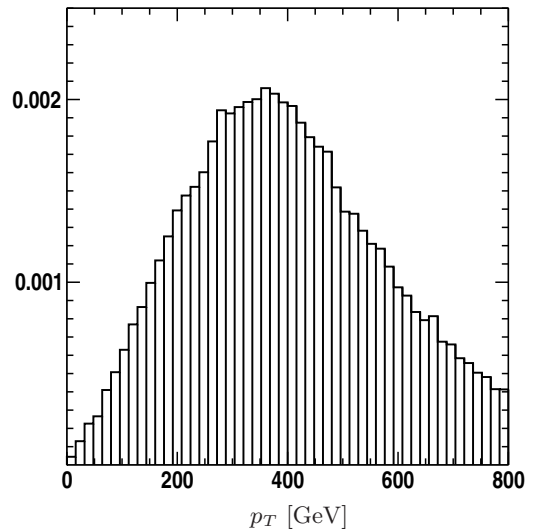


FIG. 10: p_T distribution of the top quark from the decay $\tilde{d}_R \rightarrow \mu t$ (*cf.* Table IV) at the LHC. The distribution is normalized to one.

scenarios. For example, if the decay chains of the pair produced sparticles into the $\tilde{\nu}_\mu$ LSP contain no neutrino than there is no \not{p}_T . The \not{p}_T distribution in Fig. 8 peaks at roughly 90 GeV. Thus, \not{p}_T might still be used to distinguish the SUSY signal from its SM background. Large amounts of \not{p}_T , *i.e.* \not{p}_T of a few hundred GeV, can arise if a squark decays directly via λ'_{231} into a quark and a neutrino. For example $\tilde{d}_R \rightarrow \nu_\mu b$, *cf.* Table IV. This decay also leads to a high- p_T b -jet, *i.e.* p_T of $\mathcal{O}(100 \text{ GeV})$.

Instead of high- p_T neutrinos, we can also have high- p_T muons from the direct decays of \tilde{d}_R and $\tilde{t}_{1/2}$ via λ'_{231} , see Table IV. We show in Fig. 9 the p_T distribution of these muons. The distribution peaks at 340 GeV. The

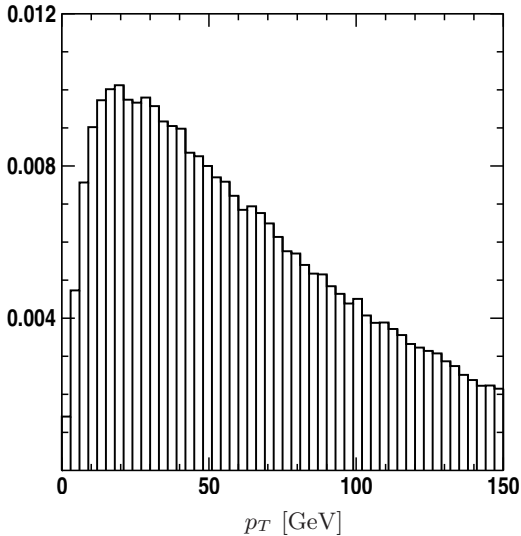


FIG. 11: p_T distribution of the muon from the decay $\tilde{\chi}_1^0 \rightarrow \tilde{\mu}_L \mu$ (cf. Table IV) at the LHC. The distribution is normalized to one.

large momenta are a consequence of the large squark masses. Nearly the entire mass of the squarks is transformed into the momenta of two SM particles. These high- p_T SM particles might also be used to reconstruct the squark mass. The muon p_T -distribution will peak at smaller values, if the squarks are lighter than in our benchmark scenario. But at the same time we will produce more squarks and muons compared to the cross section, Eq. (35). If the mass spectrum is heavier compared to our example point, the cross section will be smaller. But the muon p_T -distribution will now peak at larger values. Thus stronger cuts on the muon p_T can be applied. We conclude that the high- p_T muons might be used on the one hand to distinguish the SUSY signal from the SM background and on the other hand to distinguish the B_3 mSUGRA model with a $\tilde{\nu}_\mu$ LSP from mSUGRA with a stable $\tilde{\chi}_1^0$ LSP. For our benchmark scenario Eq. (34), we find that 11% of all sparticle pair production events lead to at least one high- p_T muon from a squark decay. A fraction of roughly 10% is a general feature of our $\tilde{\nu}_\mu$ LSP scenarios.

The neutrino or muon from the squark decay will be accompanied by a quark with roughly the opposite p_T . These quarks lead to high- p_T jets, which might be b -jets depending on the flavour indices of λ' . For our benchmark point, we obtain high- p_T b -jets from the B_3 decay $\tilde{d}_R \rightarrow \nu_\mu b$. We also can get a top-quark, t , from the decay $\tilde{d}_R \rightarrow \mu^- t$. We show in Fig. 10 the p_T -distribution of this top-quark. The distribution peaks at 360 GeV. The top decay will also produce a b -jet and a W . The W might produce additional jets or leptons with p_T . These decay products will be boosted due to the large top momentum. Thus isolated leptons can most likely not be used to reconstruct the top quark.

Finally we want to mention an effect arising from the

mass ordering in the light part of the spectrum. We have shown in Figs. 6(e), 7(e) that the $\tilde{\mu}_L$ is lighter than the $\tilde{\chi}_1^0$ in most regions of $\tilde{\nu}_\mu$ LSP parameter space allowing for the decay $\tilde{\chi}_1^0 \rightarrow \tilde{\mu}_L^\pm \mu^\mp$. Since many decay chains in Table IV involve the $\tilde{\chi}_1^0$, we expect more muons in the final state than in mSUGRA with a stable $\tilde{\chi}_1^0$ LSP [101]. For example, all right-handed squarks, which do not directly couple to the $L_2 Q_3 \bar{D}_1$ operator will predominantly decay into the $\tilde{\chi}_1^0$. Thus pair production of right-handed squarks, \tilde{q}_R , has a large fraction of the signature

$$\tilde{q}_R \tilde{q}_R \rightarrow \mu^\pm \mu^\pm jjjjjj (WW). \quad (36)$$

We have six jets, j , where two jets rise from the \tilde{q}_R decay and four jets from the decay of the two $\tilde{\mu}_L$. If the $\tilde{\mu}_L$ decay via the 3-body decay (see Table IV), two jets will be b -jets and we will also have two W s in the final state. We also find two muons from $\tilde{\chi}_1^0$ decay, where all charge combinations of the muons are possible due to the Majorana nature of the $\tilde{\chi}_1^0$. We therefore have a new source for like-sign dimuon events, which does not exist in P_6 mSUGRA scenarios with a stable $\tilde{\chi}_1^0$ LSP. In principle, it should be possible to reconstruct the full event, Eq. (36), although we have large combinatorial backgrounds due to the many jets in the final state.

We show in Fig. 11 the p_T -distribution of the muons arising from $\tilde{\chi}_1^0$ decay within our example scenario, Eq. (34). The distribution peaks at 20 GeV and therefore we expect that most of the muons will pass standard experimental cuts. However, the position of the peak is restricted by the mass difference of the $\tilde{\mu}_L$ and $\tilde{\chi}_1^0$. In our example the mass difference is 37 GeV. In general we find in Figs. 6(e), 7(e) mass differences of up to 90 GeV.

In a $\tilde{\nu}_i$ LSP scenario with $\lambda'_{ijk}|_{\text{GUT}} \neq \lambda'_{231}|_{\text{GUT}}$ we get the following differences. Now left-handed (right-handed down-type) squarks of generation j (k) will couple to the $L_i Q_j \bar{D}_k$ operator. These squarks can now decay into a quark of generation k (j) and into a lepton of generation i . In addition, the masses of these squarks will be reduced via the B_3 interaction. For $i = 1$, we have to replace the muons in the discussion above by electrons. For $i = 3$, we have taus instead of muons. We will get taus with large momenta, *i.e.* $p_\tau = \mathcal{O}(100 \text{ GeV})$, from the decays of the squarks via the B_3 interaction. These taus have a boost factor of $\gamma = \mathcal{O}(100)$ and are thus long lived leading to detached vertices of $\mathcal{O}(1 \text{ cm})$. We finally see in Figs. 7(f), 6(f) that also in large regions of $\tilde{\nu}_\tau$ LSP parameter space the $\tilde{\tau}_1$ is lighter than the $\tilde{\chi}_1^0$. This might lead to like-sign tau events from two decay chains involving a $\tilde{\chi}_1^0$.

C. Single Sparticle Production

Here we explore single sparticle production, which is not possible if P_6 is conserved. We expect high rates

process	cross section
$PP \rightarrow \tilde{\nu}_\mu + X$	2.2×10^6 fb
$PP \rightarrow \tilde{\chi}_1^0 \nu_\mu + X$	4.2×10^1 fb
$PP \rightarrow \tilde{\chi}_2^0 \nu_\mu + X$	6.2×10^0 fb
$PP \rightarrow \tilde{\chi}_1^- \mu^+ + X$	1.3×10^1 fb
$PP \rightarrow \tilde{\mu}_L^- t + X$	1.3×10^4 fb

TABLE V: Total hadronic cross sections for single sparticle production at the LHC within the $\tilde{\nu}_\mu$ LSP scenario, Eq. (34), with $\lambda'_{231}|_{\text{GUT}} = 0.11$. The cross sections include also the charge conjugated processes.

due to the large λ'_{ijk} coupling in $\tilde{\nu}_i$ LSP scenarios.

We show in Table V the hadronic cross sections for different single sparticle production processes. We again consider the example scenario, Eq. (34), with $\lambda'_{231}|_{\text{GUT}} = 0.11$. The first four cross sections are calculated with HERWIG and the last cross section is taken from Ref. [15]. The first four processes involve a real or virtual $\tilde{\nu}_\mu$, which is the LSP. The corresponding processes with the $\tilde{\mu}_L$ are not possible, because one parton in the initial state has to be a top-quark. A single $\tilde{\mu}_L$ can therefore be produced only in association with a SM particle, for example with a top-quark [15, 95], see also Table V.

We indeed observe in Table V a large cross section for the resonant production of single $\tilde{\nu}_\mu$ s due to the large λ'_{231} coupling, high parton luminosity (due to small Bjorken x) and large phase space. For 10 fb^{-1} integrated luminosity we will produce more than two million $\tilde{\nu}_\mu$ LSPs. However, the $\tilde{\nu}_\mu$ can only decay into two jets, *cf.* Table IV, where one jet is a b -jet [97, 98]. This process thus suffers from large QCD background and it will be very hard to observe an excess over the SM background at the LHC [67].

The process in Table V with the second largest cross section is single $\tilde{\mu}_L$ production in association with a top quark. This process suffers in general from the large SM $t\bar{t}$ +jet background [15]. However it might be possible to see an excess over the SM in small regions of $\tilde{\nu}_\mu$ LSP parameter space, where the $\tilde{\chi}_1^0$ is lighter than the $\tilde{\mu}_L$, *cf.* Figs. 6(e), 7(e). The $\tilde{\mu}_L$ can decay in this case to $\tilde{\chi}_1^0 \mu$ and we might employ the charge asymmetry of the muons to distinguish the signal from the background [15].

The production of a $\tilde{\chi}_1^0$ [$\tilde{\chi}_2^0$] in association with a sneutrino, Table V, can lead to a muon with jets and \cancel{p}_T in the final state, because 28% [44.8%] of the $\tilde{\chi}_1^0$ s [$\tilde{\chi}_2^0$ s] decay into a $\tilde{\mu}_L \mu$ pair. However the respective production cross sections are rather small, namely 42 fb [6.2 fb].

The production of charginos and muons, $\tilde{\chi}_1^- \mu^+$, seems more promising. Roughly 50% of the produced $\tilde{\chi}_1^-$ will decay into $\tilde{\nu}_\mu^* \mu^-$ leading to a final state with a pair of muons, and two jets, where one jet is a b -jet.

But again the cross section is small, 13 fb.

In $\tilde{\nu}_i$ LSP scenarios, where $\lambda'_{ijk}|_{\text{GUT}} \neq \lambda'_{231}|_{\text{GUT}}$, the main difference arises if $j \neq 3$. In this case also resonant single charged slepton, $\tilde{\ell}_{Li}$, production, Eq. (24), is possible via an up-type quark of generation j . Therefore, if the $\tilde{\chi}_1^0$ is lighter than the $\tilde{\ell}_{Li}$, we expect a high rate of leptons from $\tilde{\ell}_{Li}$ decay to $\tilde{\chi}_1^0 \ell_i$. But this is only possible in small regions of $\tilde{\nu}_i$ LSP parameter space, see Figs. 6(e), 6(f), 7(e) and 7(f). A further bottleneck for the observation of these leptons is the small mass difference between the $\tilde{\chi}_1^0$ and $\tilde{\ell}_{Li}$ leading to small lepton momenta. The mass difference will not exceed roughly 30 GeV. Large λ'_{ijk} couplings with $j \neq 3$ are also disfavoured by D_0 - \bar{D}_0 -mixing, *cf.* Sect. III B.

We conclude, that pair production of SUSY particles and their subsequent decays lead to much more promising signatures than single sparticle production. On the one hand, resonant single sneutrino production, which occurs at a high rate, lead mainly to jets in the final state and thus suffers from the large QCD background. On the other hand, processes with one or two leptons in the final state have small cross sections, *i.e.* $\lesssim \mathcal{O}(10 \text{ fb})$.

VI. CONCLUSION

In supersymmetric models it is essential to know the nature of the LSP, since it is involved in practically all collider signals. In the MSSM the LSP is necessarily the lightest neutralino. However, in B_3 mSUGRA models this is not the case: It had been shown previously that one can obtain a stau LSP and even a sneutrino LSP. In this paper we have analysed in detail which B_3 mSUGRA parameter region leads to a sneutrino LSP. In particular, we have found that a coupling $\lambda'_{ijk} = \mathcal{O}(10^{-1})$ at the GUT scale will lead to a sneutrino LSP due to additional B_3 terms in the RGEs. We have shown, that such a large coupling can still be consistent with experiment, for a $\tilde{\nu}_{\mu,\tau}$ LSP. A $\tilde{\nu}_e$ LSP is disfavoured due to the strong bounds on the couplings λ'_{ijk} , see Table I.

We have explored which conditions at the GUT scale lead to a sneutrino LSP. We have shown that a negative trilinear scalar coupling A_0 with a large magnitude enhances the negative B_3 contribution to the sneutrino mass. We have found large regions in the B_3 mSUGRA parameter space, where the sneutrino is the LSP and which are consistent with the observed anomalous magnetic moment of the muon, a_μ^{exp} , as well as with $\text{BR}(b \rightarrow s\gamma)$, see Figs. 6 and 7. The allowed $\tilde{\nu}_\mu$ LSP parameter space is hereby larger than the $\tilde{\nu}_\tau$ LSP parameter space. We have also shown that a_μ^{exp} puts an upper bound of roughly 300 GeV on the sneutrino LSP mass.

We have next investigated the phenomenology of sneu-

trino LSP models at the LHC. We have considered one benchmark scenario with a $\tilde{\nu}_\mu$ LSP which is obtained via $\lambda'_{231}|_{\text{GUT}} = 0.11$. Within this scenario, we have found that direct decays of light as well as heavy SUSY particles lead to an excess of muons in the final state, *cf.* Table IV. We also have found that signatures from pair production of SUSY particles are more promising than from single sparticle production, since the latter mainly involve hadronic final states. Promising pair production signatures are high- p_T muons of a few hundred GeV, *cf.* Fig. 9, high- p_T jets, like-sign muon events and long-lived taus with a detached vertex of $\mathcal{O}(1\text{cm})$.

These signatures should be investigated by the experimental groups in order to find supersymmetry as well as to distinguish B_3 mSUGRA with a sneutrino LSP from “normal” mSUGRA with a stable $\tilde{\chi}_1^0$.

Acknowledgments

We thank Benjamin Allanach for help with the as-yet unpublished B_3 version of `SOFTSUSY`. We also thank Volker Büscher for helpful discussions. SG thanks the theory groups of Fermilab National Accelerator, Argonne National Laboratory and UC Santa Cruz for helpful discussions and warm hospitality. SG also thanks the ‘Deutsche Telekom Stiftung’ and the ‘Bonn-Cologne Graduate School of Physics and Astronomy’ for financial support. This work was partially supported by BMBF grant 05 HT6PDA, by the Helmholtz Allianz HA-101 ‘Physics at the Terascale’ and by the SFB Transregio 33 ‘The Dark Universe’.

-
- [1] J. Wess and B. Zumino, Nucl. Phys. B **70** (1974) 39; M. Drees, arXiv:hep-ph/9611409; H. P. Nilles, Phys. Rept. **110** (1984) 1; S. P. Martin, arXiv:hep-ph/9709356.
 - [2] S. L. Glashow, Nucl. Phys. **22** (1961) 579; S. Weinberg, Phys. Rev. Lett. **19** (1967) 1264.
 - [3] [ATLAS Collaboration], CERN-LHCC-94-43; [CMS Collaboration], CERN-LHCC-96-45;
 - [4] H. K. Dreiner, C. Luhn and M. Thormeier, Phys. Rev. D **73** (2006) 075007 [arXiv:hep-ph/0512163].
 - [5] G. R. Farrar and P. Fayet, Phys. Lett. B **76** (1978) 575.
 - [6] J. R. Ellis, J. S. Hagelin, D. V. Nanopoulos, K. A. Olive and M. Srednicki, Nucl. Phys. B **238** (1984) 453.
 - [7] T. Hebbeker, Phys. Lett. B **470** (1999) 259 [arXiv:hep-ph/9910326].
 - [8] H. K. Dreiner, arXiv:hep-ph/9707435.
 - [9] B. C. Allanach, A. Dedes and H. K. Dreiner, Phys. Rev. D **69** (2004) 115002 [Erratum-ibid. D **72** (2005) 079902] [arXiv:hep-ph/0309196].
 - [10] B. C. Allanach, M. A. Bernhardt, H. K. Dreiner, C. H. Kom and P. Richardson, Phys. Rev. D **75** (2007) 035002 [arXiv:hep-ph/0609263].
 - [11] H. K. Dreiner and G. G. Ross, Nucl. Phys. B **365** (1991) 597.
 - [12] R. M. Godbole, P. Roy and X. Tata, Nucl. Phys. B **401** (1993) 67 [arXiv:hep-ph/9209251].
 - [13] H. K. Dreiner, P. Richardson and M. H. Seymour, Phys. Rev. D **63**, 055008 (2001) [arXiv:hep-ph/0007228].
 - [14] A. Bartl, W. Porod, D. Restrepo, J. Romao and J. W. F. Valle, Nucl. Phys. B **600** (2001) 39 [arXiv:hep-ph/0007157].
 - [15] M. A. Bernhardt, H. K. Dreiner, S. Grab and P. Richardson, Phys. Rev. D **78** (2008) 015016 [arXiv:0802.1482 [hep-ph]].
 - [16] B. C. Allanach, M. A. Bernhardt, H. K. Dreiner, S. Grab, C. H. Kom and P. Richardson, arXiv:0710.2034 [hep-ph].
 - [17] H. K. Dreiner, J. Soo Kim and M. Thormeier, arXiv:0711.4315 [hep-ph].
 - [18] H. K. Dreiner, S. Grab and M. K. Trenkel, arXiv:0808.3079 [hep-ph].
 - [19] A. G. Akeroyd, M. A. Diaz, J. Ferrandis, M. A. Garcia-Jareno and J. W. F. Valle, Nucl. Phys. B **529** (1998) 3 [arXiv:hep-ph/9707395]; A. G. Akeroyd, C. Liu and J. H. Song, Phys. Rev. D **65** (2002) 015008 [arXiv:hep-ph/0107218].
 - [20] N. Sakai and T. Yanagida, Nucl. Phys. B **197** (1982) 533; S. Weinberg, Phys. Rev. D **26** (1982) 287.
 - [21] B. C. Allanach, A. Dedes and H. K. Dreiner, Phys. Rev. D **60** (1999) 075014 [arXiv:hep-ph/9906209].
 - [22] S. Dimopoulos, S. Raby and F. Wilczek, Phys. Lett. B **112** (1982) 133; A. Y. Smirnov and F. Vissani, Phys. Lett. B **380** (1996) 317 [arXiv:hep-ph/9601387]; G. Bhattacharyya and P. B. Pal, Phys. Rev. D **59** (1999) 097701 [arXiv:hep-ph/9809493].
 - [23] R. Barbier *et al.*, Phys. Rept. **420** (2005) 1 [arXiv:hep-ph/0406039].
 - [24] M. Shiozawa *et al.* [Super-Kamiokande Collaboration], Phys. Rev. Lett. **81** (1998) 3319 [arXiv:hep-ex/9806014].
 - [25] L. E. Ibanez and G. G. Ross, Phys. Lett. B **260** (1991) 291; L. E. Ibanez and G. G. Ross, Nucl. Phys. B **368** (1992) 3.
 - [26] H. S. Lee, K. T. Matchev and T. T. Wang, Phys. Rev. D **77** (2008) 015016 [arXiv:0709.0763 [hep-ph]]; H. S. Lee, C. Luhn and K. T. Matchev, JHEP **0807** (2008) 065 [arXiv:0712.3505 [hep-ph]]; H. S. Lee, Phys. Lett. B **663** (2008) 255 [arXiv:0802.0506 [hep-ph]].
 - [27] H. E. Haber, Nucl. Phys. Proc. Suppl. **62** (1998) 469 [hep-ph/9709450].
 - [28] A. H. Chamseddine, R. Arnowitt and P. Nath, Phys. Rev. Lett. **49** (1982) 970; L. Alvarez-Gaume, M. Claudson and M. Wise, Nucl. Phys. B **207** (1982) 96; L. Ibanez, Phys. Lett. B **118** (1982) 73; S. K. Soni and H. A. Weldon, Phys. Lett. B **126** (1983) 215; L. J. Hall, J. D. Lykken and S. Weinberg, Phys. Rev. D **27** (1983) 2359; R. Barbieri, S. Ferrara and C. A. Savoy, Phys. Lett. B **119** (1982) 343.
 - [29] L. E. Ibanez and G. G. Ross, Phys. Lett. B **110**

- (1982) 215.
- [30] M. Drees and S. P. Martin, arXiv:hep-ph/9504324.
- [31] L. E. Ibanez, C. Lopez and C. Munoz, Nucl. Phys. B **256** (1985) 218.
- [32] J. F. Gunion and H. E. Haber, Nucl. Phys. B **272** (1986) 1 [Erratum-ibid. B **402** (1993) 567].
- [33] I. Jack, D. R. T. Jones and A. F. Kord, Phys. Lett. B **632** (2006) 703 [arXiv:hep-ph/0505238].
- [34] B. C. Allanach, H. K. Dreiner, P. Morawitz and M. D. Williams, Phys. Lett. B **420** (1998) 307 [arXiv:hep-ph/9708495].
- [35] S. Dimopoulos and L. J. Hall, Phys. Lett. B **207** (1988) 210; H. K. Dreiner, P. Richardson and M. H. Seymour, Phys. Rev. D **63** (2001) 055008 [arXiv:hep-ph/0007228]; G. Moreau, E. Perez and G. Polesello, Nucl. Phys. B **604** (2001) 3 [arXiv:hep-ph/0003012]; V. M. Abazov *et al.* [D0 Collaboration], Phys. Rev. Lett. **97** (2006) 111801 [arXiv:hep-ex/0605010]; D. Choudhury, S. Majhi and V. Ravindran, Nucl. Phys. B **660** (2003) 343 [arXiv:hep-ph/0207247]; L. L. Yang, C. S. Li, J. J. Liu and Q. Li, Phys. Rev. D **72** (2005) 074026 [arXiv:hep-ph/0507331]; Y. Q. Chen, T. Han and Z. G. Si, JHEP **0705** (2007) 068 [arXiv:hep-ph/0612076].
- [36] H. K. Dreiner, S. Grab, M. Krämer and M. K. Trenkel, Phys. Rev. D **75** (2007) 035003 [arXiv:hep-ph/0611195].
- [37] B. C. Allanach *et al.*, arXiv:hep-ph/0202233.
- [38] B.C. Allanach and M.A. Bernhardt, unpublished.
- [39] F. Gabbiani, E. Gabrielli, A. Masiero and L. Silvestrini, Nucl. Phys. B **477** (1996) 321 [arXiv:hep-ph/9604387]; S. Jager, arXiv:0808.2044 [hep-ph].
- [40] K. Agashe and M. Graesser, Phys. Rev. D **54** (1996) 4445 [arXiv:hep-ph/9510439].
- [41] B. de Carlos and P. L. White, Phys. Rev. D **54** (1996) 3427 [arXiv:hep-ph/9602381].
- [42] H. K. Dreiner and H. Pois, arXiv:hep-ph/9511444.
- [43] V. D. Barger, M. S. Berger, R. J. N. Phillips and T. Wohrman, Phys. Rev. D **53** (1996) 6407 [arXiv:hep-ph/9511473].
- [44] E. Nardi, Phys. Rev. D **55** (1997) 5772 [arXiv:hep-ph/9610540].
- [45] L. J. Hall and M. Suzuki, Nucl. Phys. B **231** (1984) 419.
- [46] J. R. Ellis, G. Gelmini, C. Jarlskog, G. G. Ross and J. W. F. Valle, Phys. Lett. B **150** (1985) 142.
- [47] T. Banks, Y. Grossman, E. Nardi and Y. Nir, Phys. Rev. D **52** (1995) 5319 [arXiv:hep-ph/9505248].
- [48] D. N. Spergel *et al.* [WMAP Collaboration], Astrophys. J. Suppl. **148** (2003) 175 [arXiv:astro-ph/0302209].
- [49] M. Colless *et al.*, arXiv:astro-ph/0306581.
- [50] M. Chemtob, Prog. Part. Nucl. Phys. **54** (2005) 71 [arXiv:hep-ph/0406029]; H. K. Dreiner, M. Krämer and B. O'Leary, Phys. Rev. D **75** (2007) 114016 [arXiv:hep-ph/0612278].
- [51] A. A. Petrov and G. K. Yeghiyan, Phys. Rev. D **77** (2008) 034018 [arXiv:0710.4939 [hep-ph]].
- [52] E. Golowich, J. Hewett, S. Pakvasa and A. A. Petrov, Phys. Rev. D **76** (2007) 095009 [arXiv:0705.3650 [hep-ph]].
- [53] B. Aubert *et al.* [BABAR Collaboration], Phys. Rev. D **76** (2007) 014018 [arXiv:0705.0704 [hep-ex]].
- [54] B. Aubert *et al.* [BABAR Collaboration], Phys. Rev. Lett. **98** (2007) 211802 [arXiv:hep-ex/0703020].
- [55] K. Abe *et al.* [BELLE Collaboration], Phys. Rev. Lett. **99** (2007) 131803 [arXiv:0704.1000 [hep-ex]].
- [56] M. Staric *et al.* [Belle Collaboration], Phys. Rev. Lett. **98** (2007) 211803 [arXiv:hep-ex/0703036].
- [57] T. Aaltonen *et al.* [CDF Collaboration], Phys. Rev. Lett. **100** (2008) 121802 [arXiv:0712.1567 [hep-ex]].
- [58] A. J. Schwartz, arXiv:0803.0082 [hep-ex].
- [59] L. Wolfenstein, Phys. Rev. Lett. **51** (1983) 1945; J. Charles *et al.* [CKMfitter Group], Eur. Phys. J. C **41**, 1 (2005) [arXiv:hep-ph/0406184].
- [60] G. Abbiendi *et al.* [OPAL Collaboration], Eur. Phys. J. C **33** (2004) 149 [arXiv:hep-ex/0310054].
- [61] A. Heister *et al.* [ALEPH Collaboration], Eur. Phys. J. C **31** (2003) 1 [arXiv:hep-ex/0210014].
- [62] M. Wendel and H. Fraas, Phys. Rev. D **44** (1991) 60.
- [63] B. C. Allanach, S. Kraml and W. Porod, JHEP **0303** (2003) 016 [arXiv:hep-ph/0302102].
- [64] G. Degrassi, S. Heinemeyer, W. Hollik, P. Slavich and G. Weiglein, Eur. Phys. J. C **28** (2003) 133 [arXiv:hep-ph/0212020].
- [65] B. C. Allanach, A. Djouadi, J. L. Kneur, W. Porod and P. Slavich, JHEP **0409** (2004) 044 [arXiv:hep-ph/0406166].
- [66] R. Barate *et al.*, Phys. Lett. B **565** (2003) 61 [arXiv:hep-ex/0306033].
- [67] J. L. Hewett and T. G. Rizzo, arXiv:hep-ph/9809525.
- [68] V. M. Abazov *et al.* [D0 Collaboration], Phys. Rev. D **69** (2004) 111101 [arXiv:hep-ex/0308033].
- [69] F. Abe *et al.* [CDF Collaboration], Phys. Rev. Lett. **74**, 3538 (1995) [arXiv:hep-ex/9501001].
- [70] F. Abe *et al.* [CDF Collaboration], Phys. Rev. D **55** (1997) 5263 [arXiv:hep-ex/9702004].
- [71] CDF Collaboration, CDF note 9246
- [72] D0 Collaboration, D0 note 4403-CONF
- [73] W. M. Yao *et al.* [Particle Data Group], J. Phys. G **33** (2006) 1.
- [74] H. K. Dreiner and R. J. N. Phillips, Nucl. Phys. B **367** (1991) 591.
- [75] A. Belyaev, M. H. Genest, C. Leroy and R. R. Mehdiev, JHEP **0409** (2004) 012 [arXiv:hep-ph/0401065].
- [76] G. Eilam, A. Gemintern, T. Han, J. M. Yang and X. Zhang, Phys. Lett. B **510** (2001) 227 [arXiv:hep-ph/0102037].
- [77] K. J. Abraham, K. Whisnant, J. M. Yang and B. L. Young, Phys. Rev. D **63** (2001) 034011 [arXiv:hep-ph/0007280].
- [78] D. K. Ghosh, S. Raychaudhuri and K. Sridhar, Phys. Lett. B **396** (1997) 177 [arXiv:hep-ph/9608352].
- [79] K. I. Hikasa, J. M. Yang and B. L. Young, Phys. Rev. D **60** (1999) 114041 [arXiv:hep-ph/9908231].
- [80] P. Y. Li, G. R. Lu, J. M. Yang and H. Zhang, Eur. Phys. J. C **51** (2007) 163 [arXiv:hep-ph/0608223].
- [81] J. Alitti *et al.* [UA2 Collaboration], Z. Phys. C **49** (1991) 17.
- [82] J. Alitti *et al.* [UA2 Collaboration], Nucl. Phys. B **400** (1993) 3.
- [83] D. Stockinger, arXiv:0710.2429 [hep-ph].
- [84] J. P. Miller, E. de Rafael and B. L. Roberts, Rept. Prog. Phys. **70** (2007) 795 [arXiv:hep-ph/0703049].
- [85] G. W. Bennett *et al.* [Muon G-2 Collaboration], Phys. Rev. D **73** (2006) 072003 [arXiv:hep-ex/0602035].

- [86] J. A. Grifols and A. Mendez, Phys. Rev. D **26** (1982) 1809.
- [87] D. Stockinger, J. Phys. G **34** (2007) R45 [arXiv:hep-ph/0609168].
- [88] J. E. Kim, B. Kyae and H. M. Lee, Phys. Lett. B **520** (2001) 298 [arXiv:hep-ph/0103054].
- [89] E. Barberio *et al.* [Heavy Flavor Averaging Group], arXiv:0808.1297 [hep-ex].
- [90] P. Gambino and M. Misiak, Nucl. Phys. B **611** (2001) 338 [arXiv:hep-ph/0104034]; A. J. Buras, A. Czarnecki, M. Misiak and J. Urban, Nucl. Phys. B **631** (2002) 219 [arXiv:hep-ph/0203135].
- [91] G. Belanger, F. Boudjema, A. Pukhov and A. Semenov, Comput. Phys. Commun. **149** (2002) 103 [arXiv:hep-ph/0112278].
- [92] G. Corcella *et al.*, JHEP **0101** (2001) 010 [arXiv:hep-ph/0011363]; G. Corcella *et al.*, arXiv:hep-ph/0210213; S. Moretti, K. Odagiri, P. Richardson, M. H. Seymour and B. R. Webber, JHEP **0204** (2002) 028 [arXiv:hep-ph/0204123].
- [93] The version of HERWIG [92] used in this paper includes modifications to simulate the four-body decays of a stau LSP and was implemented by Peter Richardson.
- [94] F. E. Paige, S. D. Protopopescu, H. Baer and X. Tata, arXiv:hep-ph/0312045.
- [95] F. Borzumati, J. L. Kneur and N. Polonsky, Phys. Rev. D **60** (1999) 115011 [arXiv:hep-ph/9905443]; E. Accomando *et al.*, arXiv:hep-ph/0608079; A. Belyaev, M. H. Genest, C. Leroy and R. R. Mehdiev, JHEP **0409** (2004) 012 [arXiv:hep-ph/0401065].
- [96] We use as SM inputs for SOFTSUSY the following parameters: $M_Z = 91.1876$ GeV ($m_t = 172.5$ GeV) for the pole mass of the Z boson (top quark); $\alpha^{-1}(M_Z) = 127.918$ and $\alpha_s(M_Z) = 0.1187$ for the gauge couplings in the \overline{MS} scheme; $m_b(m_b) = 4.25$ GeV, $m_u(2\text{GeV}) = 0.003$ GeV, $m_d(2\text{GeV}) = 0.00675$ GeV, $m_s(2\text{GeV}) = 0.1175$ GeV and $m_c(m_c) = 1.2$ GeV for the light quark masses in the \overline{MS} scheme.
- [97] The $\tilde{\nu}_\mu$ LSP might also decay via a 4-body decay, *e.g.* $\tilde{\nu}_\mu \rightarrow \nu_\mu \bar{\nu}_\mu d \bar{b}$, via a virtual neutralino and sneutrino. However we estimate that the 4-body decay rates are suppressed by eight orders of magnitude compared to the 2-body decay. We employed the analytical formulæ of Ref. [9].
- [98] The $\tilde{\nu}_\mu$ can in principle also decay via a RGE generated λ_{121} (λ_{323}) coupling into a $e\nu_e$ ($\tau\nu_\tau$) pair. However the generated λ 's are at least ten orders of magnitude smaller than the λ'_{231} coupling. The relevant RGEs to generate the λ s involve off-diagonal down-Yukawa matrix elements, which vanish at M_Z , see Sect. III A.
- [99] In general, also $\mathbf{\Lambda} \in \{\lambda_{ijk}\}$ at M_{GUT} is allowed in B_3 mSUGRA models. $\kappa_i|_{\text{GUT}}$ is rotated away; see Ref. [9] for details.
- [100] For $i = 3$, we also have terms proportional to $(\mathbf{Y}_E)_{33}^2$, *i.e.* proportional to the tau Yukawa coupling squared.
- [101] Note, that also the $\tilde{\chi}_2^0$ and $\tilde{\chi}_1^-$ decay to a muon with a BR of roughly 50%, see Table IV.